PERMEABILITY MEASUREMENTS OF COMPRESSIBLE, POROUS MEDIA

by

MAURA ELIZABETH DONNELLY

B.S.M.E., Tufts University

(1980)

SUBMITTED TO THE DEPARTMENT OF
MECHANICAL ENGINEERING IN
PARTIAL FULFILLMENT OF THE
REQUIREMENTS FOR THE
DEGREE OF

MASTER OF SCIENCE

at the

MASSACHUSETTS INSTITUTE OF TECHNOLOGY

June 1982

Signature of Author _____
Department of Mechanical Engineering

Certified by _____

Roger D. Kamm
Thesis Supervisor

Accepted by _____

Warren Rohsenow
Chairman, Department Committee on Graduate Studies

PERMEABILITY MEASUREMENTS OF COMPRESSIBLE,POROUS MEDIA

by

MAURA ELIZABETH DONNELLY

Submitted to the Department of Mechanical Engineering
on May 29,1982 in partial fulfillment of the
requirements for the Degree of Master of Science.

ABSTRACT

Permeability of compressible porous media can be measured experimentally by two methods:

1.) Flow experiments based on Darcy's law
2.) Optical methods based on Kozeny's analysis

In this study, we establish the validity of the optical method as a means of determining the permeability of porous media from their photomicrographs.

Flow experiments involving extension and compression of the foams are performed and permeabilities are calculated. These values are compared to the permeabilities obtained by analyzing photomicrographs of the same foam using an Apple computer with a graphics tablet.

The major conclusions which can be reached based on the results obtained are:

1.) The optical method used to determine permeability does give accurate results.
2.) Permeability is a function of compression ratio (relative change of length of the sample). Flow-induced and external compression decrease compression ratio and hence decrease permeability, while flow extension acts in the opposite manner.

Thesis Supervisor: Roger D. Kamm
Title: Associate Professor of Mechanical Engineering

ACKNOWLEDGEMENTS

First, I would like to thank Professor Roger Kamm for giving me the chance to work on such an interesting problem. His guidance was always appreciated. I am also grateful to my colleagues on the project: Jason, Bryan, and Mark for their suggestions and insights. Thanks to the members of the Howe Laboratory at Mass. Eye and Ear Infirmary for our monthly meetings which proved to be of great value. Special thanks to Dr. Don Pihlaja for his invaluable assistance in preparing my foam samples and to Prof. Dewey for the use of his Apple computer.

Next, I thank Dick Fenner for his help in keeping my experiment in one piece. Without his help, I would still be swimming in a sea of silicon oil!

I want to thank my friends and lab-mates for making my experience at M.I.T. so enjoyable. To Suzy, Rich, Watts, Opus, and Jan go my special love and appreciation.

Finally, I thank my mother. She always encouraged me to do my best and for that I am ever grateful.

This work was funded by the National Institute of Health (Grant No.1 R01 EY 03141-01)

TABLE OF CONTENTS

CHAPTER 1

INTRODUCTION

The analysis of the hydrodynamics of flow through porous media has traditionally been of interest to petroleum engineers (Muscat),hydrologists (Bear), chemical engineers and other scientists. (Dickey, Terzaghi, Pryor) There are a number of natural and industrial processes which involve flow through a porous material in which the material may be deformed by the forces associated with the flow. The drying of textiles,the cooling of germinating malt beds, and the seepage of water through the earth around a resevoir are possible examples.In these cases, the fluid flow and the deformation of the permeable media are coupled, and any analysis of the problem requires the simultaneous solution of the flow and deformation equations.

One of the first of many analyses for the fluid flow within a deformable porous medium was due to Biot (1941) He considered the deformation of liquid-saturated materials within the scope of infinitesimal elastic strain theory. Since then, numerous analytical studies have been conducted in an attempt to understand this flow situation. Many of these are quite complex and often require a thorough knowledge of parameters characterizing the pore structure.

Several different models have been used to describe the porous material involved. The most common and simplest of these is the cylindrical tube model,where the pore structure is modelled as a cylindrical capillary of such length and diameter that it exhibits the same resistance to flow as the actual interstices in the real porous medium.(Ergun, Sheffield)

The fact is, however, that actual pores are not isolated circular cylinders of constant cross sectional area,rather they are interconnected and often non-circular and later models have tried to account for this.(Dullien)

1.1 Analysis by Beavers et al

One of the most recent and significant studies on compressible porous media was done by Beavers,Hajji,and Sparrow. It deals with steady, one-dimensional flow of a non-compressible fluid through a highly compressible material. The analysis is not restricted to small deformations or flow within the Darcy regime (i.e. low velocity flow). Beavers and coworkers observed that the gradient of the stress within the porous media (σ) is of equal and opposite magnitude to the fluid pressure gradient established in the flow:

$$\frac{d\sigma}{dx} = \frac{dp}{dx} \qquad \text{Eq. 1.1}$$

By incorporating this into the Darcy-Forcheimer relationship for flow through porous media:

$$\frac{dp}{dx} = -p + \frac{\mu U}{k} + \frac{c\rho U^2}{\sqrt{k}}$$

Eq. 1.2

where p is opening pressure

μ is viscosity

k is permeability

U is superficial velocity

c is Forcheimer coefficient

ρ is density

they were able to develop an expression which ,when integrated, can be used to compute the mass flow rate vs. stress across a finite length sample of porous material(L_o).

$$L_o = \int_0^{\lambda} \frac{\frac{d\sigma}{d\lambda}\, d\lambda}{-P + \frac{\mu}{k\rho A}\dot{m} + \frac{c}{\sqrt{k}\rho A^2}\dot{m}^2}$$

Eq. 1.3

where A is flow area

$\dot{m}$ is mass flow rate

Beavers et al conducted a series of experiments to verify this theory using polyurethane foam rubber as the compressible medium. The stress induced within the material was applied externally by means of a movable platform. Two different fluids, air and water,were used and mass flow rate and pressure drop across the sample were measured. Stress-deformation data was also obtained for each foam type. Some typical results are presented in figure 1. Beavers obtained good agreement between predicted values of and m and those measured experimentally.

The field of study of compressible porous media is

far from being totally explored . It should be noted again that even Beavers' analysis is limited to the case of steady, one-dimensional ,non-compressible fluid flow. A further limitation is that this theory does not apply to very low porosity media. Finally, his permeability/ strain relationship had to be determined by experiment ,which makes a strict analytical solution impossible. However, all of these analyses provide valuable information from which to develop new theories for flow through porous media.

Recently, a new group of scientists have embraced the classical study of porous media with the hope of explaining a very different type of problem.Biomedical engineers are now using the same basic principles developed by Darcy and Kozeny to examine fluid flow through biological tissue. A specific application in this area is the study of the flow of aqueous humor through the trabecular meshwork of the eye as part of an effort to understand glaucoma.

1.2 Open angle glaucoma

Open angle glaucoma is caused by an increase in the intraocular pressure (I.O.P.) produced by a high resistance to flow through the aqueous outflow network (fig. 2). In the human eye, aqueous humor is formed in the ciliary processes behind the iris. From here it flows into the posterior chamber, in front of the lens, and then through the pupil to the anterior chamber. The aqueous continues to flow through the trabecular meshwork and into Schlemm's canal, where it then dumps into collector channels which lead to the aqueous

veins. At this point it is reabsorbed into the blood stream.

The pressure drop across the entire network is 7mm. Hg for the normal human eye. In glaucoma this rises dramatically, and can sometimes exceed 40 mm. Hg. Since the flow rate of aqueous humor remains nearly constant, the resistance in the outflow network of the glaucomatous eye is higher than that of the normal eye.

The question of where and how this flow resistance is produced has not been answered satisfactorily. Collapse of the aqueous veins and of Schlemm's canal have been investigated as two possible mechanisms, but both have been shown to be incapable of producing such a significant increase in the I.O.P. (Battaglioli,Johnson) Current evidence supports the hypothesis that changes in the juxtacanalicular meshwork are responsible for the large values of resistance (Chaudry et al). Therefore, it would be helpful to examine this structure of the eye more closely.

1.3 Trabecular Meshwork (Fig. 3)

One of the first classical descriptions of the trabecular meshwork was given by Salzmann in 1912. He described the meshwork as a three-sided prismatic band; anteriorly the edge is extremely sharp and unites with Descemet's membrane and the adjacent corneal lamellae; posteriorly trabeculae extend to unite with the scleral spur, the anterior surface of the ciliary body and indirectly with the root of the iris; the outer surface

borders directly upon corneal and scleral tissue and upon the inner wall of Schlemm's canal or the loose tissue surrounding it; the inner surface is free and is in contact with the aqueous humor of the anterior chamber(Ashton,Brini,Smith)

The meshwork itself consists of a series of graded porous sheets and is generally divided into two segments:

1.) Uveal meshwork

2.) Corneo-scleral meshwork , which includes the endothelial meshwork

The uveal meshwork is located adjacent to the anterior chamber and terminates in the ciliary body and root of the iris. It is made up of fibrous trabeculae of circular cross section (5μm in diameter) which are loosely connected to form highly porous sheets. There are a total of 3-5 layers with a total width of 20μm. The inner two sheets are predominantly radially-disposed, while the outer sheets are circumferentially oriented- parallel to the limbus. (Tripathi)

The corneo-scleral meshwork is situated next to Schlemm's canal. It is connected posteriorly to the scleral spur and anteriorly it extends into the deeper corneal layers to the sclera. It consists of approximately 8-15 layers of woven fibrous trabeculae.

A comparison of these two elements shows that the uveal meshwork is more porous than the corneo-scleral meshwork. Intratrabecular spaces in the former vary in size

from 25-75 μm in cross-section. The openings progressively decrease in size and in the deeper layer of the corneo-scleral meshwork they are about 2-15 μm.

The final segment of the trabecular meshwork is actually a sub-division of the corneo-scleral region, known as the endothelial meshwork. This is the region between the basal aspect of the endothelial lining of Schlemm's canal and the first layer of the corneo-scleral trabeculae. The cells of this structure are arranged with their long axes parallel to the endothelium lining the canal and form a network of long interlacing processes. The extracellular spaces here are fewer than in the remainder of the corneo-scleral meshwork. (Grierson,Lee)

1.4 Ground Substance

All of the interstitial spaces in the trabecular meshwork are filled with ground substance. Although the exact nature and composition of this ground substance are not known, we might expect it to be a two-phase system: a gel-like phase composed of glycosaminoglycan and a free-fluid phase which contains plasma proteins. In addition there exist numerous fibers of both elastin and collagen. One of the mucopolysacchrides found in the ground substance is hyaluronic acid. This is a linear polymer of N-acetylglucosamine and glucaronic acid which has a molecular weight of 2.5x10*6. It has a diameter of 8 Å and a length of 1 μm (Welderhielm et al).

Normally, the system is in osmotic equilibrium.

However, hyaluronic acid can undergo changes in its physical state due to its gel-like nature. The partition between fluid and gel phases shifts with a change in the concentration of some of its components, specifically albumin and hyaluronate. Welderhielm et al (1976) showed that an increase in hyaluronate will cause a increase in the excluded fluid volume in gel phase; whereas an increase in albumin will cause a decrease of fluid in the gel phase.

Obviously, the presence of ground substance in the trabecular meshwork will affect the flow characteristics of aqueous humor. Preston has estimated that the flow of water in a vertical capillary tube of .1mm. diameter containing a 1 cm. thickness hyaluronic acid gel will encounter a flow resistance 1000 times greater than the flow through the same tube without the gel. In fact, it has been shown that hyaluronidase, the enzyme which strips hyaluronic acid, does increase the water conductance of corneal stroma by 50 fold (Hedbys, Mishima). However, the same substantial change has not been observed in the meshwork. The total role of the ground substance and its effect on flow through the trabecular meshwork is not entirely known but it is necessary to include this in any model of the meshwork.

As early as 1908, a theory has existed that an increase in flow resistance could be caused by narrowing of the intratrabecular spaces by some foreign substance (Henderson). In order to explore this line of thought , it would be helpful to have quantitative measurements of the

meshwork permeability,which is inversely proportional to the resistance, as well as detailed information on the nature of the flow of aqueous humor.

1.5 Goals/Rationale

The porous nature of the meshwork suggests that the use of classical methods of analysis of porous media would be beneficial in characterizing the flow. However, it should be pointed out that the comparison of the trabecular meshwork to a porous medium has severe limitations. The meshwork differs from a porous medium such as foam, for example, in many ways. The porosity of the meshwork in the endothelial region, i.e. the ratio of void volume to bulk volume, is much smaller than that of most commercial open-cell foams which have a porosity in the range of .8-.95. Also, since the porosity of the meshwork is graded, separate analyses must be made for each of the distinct regions. The meshwork is living tissue, and active physiological processes occur which may have an effect on the flow. It is highly anisotropic ,consisting of sheets of interwoven beams, as compared to foam, which is generally isotropic.

With these limitations in mind, a study of compressible porous media will be undertaken. The experiments will be directed towards measuring the undeformed permeability of a polyurethane foam and also towards study of the effect of flow-induced extension and two modes of compression on this permeability. Qualitative

observations will be made on the nature of the flow through the porous media and indirectly on the flow through the trabecular meshwork of the eye.

CHAPTER 2

MEASUREMENTS OF FOAM MICROSCOPIC GEOMETRY AND ELASTIC PROPERTIES

The goals of these experiments were:

1.)to examine the flow characteristics of one or more compressible porous media

2.)to determine the undeformed permeability of the porous media

3.)to assess the effect of flow extension and compression of the foam on its permeability

2.1 Selection of the porous media

While the emphasis of the work was placed on the study of porous media, it was desirable to analyze samples that had some superficial structural similarities to the trabecular meshwork. This would allow for qualitative conclusions to be drawn between flow through porous media and flow through the trabecular meshwork. Therefore, a material was sought which was open-celled, highly deformable and, if possible, with a low porosity. The porous media finally chosen was polyurethane foam because it satisfies the necessary requirements.

An attempt was made to manufacture the desired foam using Hypol hdrophylic polyurethane prepolymer. The density and compressive strength of this foam could be controlled by

adjusting the amount of water and catalysts which were mixed with the prepolymer to create the foam. Ideally, it would be possible to produce a very dense open cell foam which was of the type desired. However, the experiments in foam production were unsuccessful. Achieving a homogenous mix of ingredients before the foaming reaction began was difficult, even when mechanically combined. As a result the foam was highly porous and had a high degree of anisotropy. This made it unsuitable for use in experimentation.

The alternative was to find a commercially produced polyurethane foam. This proved to be satisfactory, but it was impossible to find a foam dense enough to closely simulate the meshwork. This was one of the limitations of the experiments.

Two gray polyurethane ester foams were chosen as the test media. One had a density of 2 p.c.f. (pounds/cubic foot) . The other was a 6 p.c.f. foam. It was assumed that the two foams were of sufficiently different porosity and permeability to give a range of results.

2.2 Scanning electron micrographs of the polyurethane foam

The first step in the experiments, once suitable test media were obtained, was to characterize the phsical structure and geometry of the foam. For this purpose, scanning electron micrographs were taken of each foam at a magnification of 30X for the 6 p.c.f. foam and 20X for the 2 p.c.f. foam. Sample photographs of both the 2 p.c.f. and 6 p.c.f. foam are shown in figures 4 and 5. It can be seen in

the photographs of the 2 p.c.f. foam that the pores are irregularly shaped. A majority are pentagonal. They appear to be formed by interweaving of fibrous beams as opposed to being openings in a solid material. The average beam width for this foam is approximately 42 μm. An interesting feature of this picture is the existence of a thin film coating which totally or partially covers several of the pores. This would seem to be an artifact of the manufacturing process. It should be noted that this film does occlude some of the flow area and hence could decrease the effective flow area and the porosity. This reduction would decrease the measured permeability and could be a source of some slight experimental error.

The 6 p.c.f. foam, shown in fig. 5 also appears to be constructed of the same beam-like fibers. The beam thickness is roughly the same of that of the 2 p.c.f. foam. The pores are more rounded than the pores in the 2 p.c.f. foam. One similarity is the presence of the same film coating over some of the pores. This appears to be even more prevalent in the 6 p.c.f. foam.

Figures 6 and 7 show both foams as they would appear without the film coating. These pictures were obtained using back scattered light with scanning electron microscopy.

Due to the highly three dimensional appearance of these photos, they were not suitable for making quantitative measurements of the foam. Transmission micrography was used to obtain magnified pictures of the foam in two dimensions.

The procedure is outlined below.

2.3 Embedding and photographic techniques

Small cubes of foam, measuring 5 mm. on each side were placed in gelatin capsules and infiltrated with an epoxide resin known as Epon 812 . Prior to being set, the foam was coated with gold dust. This was done to facilitate the removal of trapped air from within the foam samples. Once the cubes were immersed in Epon, they were placed in a vacuum for 24 hours to further insure that no air remained inside. The capsules were then allowed to cure in a 60C oven for 2-3 days until completely hard.

From these set pieces it was possible to obtain two dimensional cross sectional representations of the foam. This was done by slicing the foam with a Reichert sledge microtome equipped with a Reichert-Jung 16 cm. stainless steel knife which was capable of cutting slices to a thickness of 1μm. Slices of 30-40 μm were of sufficient thickness to give a view of a random plane within the foam. Since the foam was considered to be isotropic, it was not necessary to maintain a specific orientation when cutting.

Next, the slices were examined using a Reichert Zetopan microscope equipped with a 5.5/.15 epi lens and 6.3X magnifying eyepieces. Overhead light was supplied by a Sorensen zenon lamp. They were then photographed at 32x magnification using a Polaroid Land Back CB-100 camera which was attached to the scope. Sample photographs are shown in figs. 8 and 9.

The 2 p.c.f. foam appears as a collection of foam wall fractions. In some cases, enclosed pores are discernible. The 6 p.c.f. sample is seen to be more dense and there are a larger number of enclosed connected pores.

2.4 Porosity and specific surface

Porous media can be characterized by a number of geometrical properties. Two parameters that are of importance are porosity and specific surface. Porosity is defined as the ratio of void volume to total volume. Specific surface is the ratio of internal pore area to the bulk volume. The quantitative analysis of photomicrographs involves the use of empirical correlations which relate these parameters to permeability.

Optical methods of determining porosity and specific surface have been widely used for the past fifty years. Porosity measurements using photomicrographs were performed by Zvodoskaya (1937) on porcelain and Verbeck (1949) on concrete. Chalkey (1949) used a stochastic method based on dropping a pin onto a picture of a porous medium. If the point landed within a void space, then it was scored as a hit. The porosity of a specimen could then be computed knowing the number of throws and hits. Specific surface can also be determined from photographs by measuring the ratio of the circumference of pores to the total area of the section. Chalkey was also able to measure specific surface using the same basic statistical method. He measured hits, throws and cuts. A cut was scored if the needle intersected

the perimeter of the pore. The specific surface is then computed as:

$$S = \frac{4Pc}{rh}$$

where: c is # of cuts
h is # of hits
r is pin length

A new and potentially more powerful way of measuring specific surface and porosity is provided by the use of a mini-compputer equipped with a digitizing pad. It was this technique which was used to analyze the photomicrographs of the polyurethane foam.

2.5 Experimental analysis of photomicrographs

The computer used in these experiments was an Apple II Plus with a graphics tablet. The tablet is a device which converts the position and movement of an indicator pen on a magnetic surface into digital data which can be processed using canned software. The experiments conducted are detailed below.

The Apple graphics tablet consists of a magnetic high resolution screen that measures 27.94 cm. x 25.4 cm. and two rows of command functions which can be activated by touching the appropriate box with the indicator pen. The resolution of the tablet could be controlled by adjusting its DELTA setting. This function has a default value of .2 cm., i.e. the tablet will draw a line each time the pen is moved a vertical or horizontal distance of .2 cm.

The procedure for measuring pictures is as follows. A polaroid black and white photomicrograph (8.13 cm. x 10.68 cm.) was taped onto the tablet's surface. The tablet was then calibrated to output measurements in centimeters using

the CALIBRATE command. A distance of 26 screen units corresponded to 2.54 cm. This was divided by 32 to account for photo magnification.

Area measurements were taken by first pressing the AREA square and then tracing a pore or wall fraction with the indicator pen. The computer would flash the area onto the screen in about five seconds. The same procedure was followed to measure perimeter except that the DISTANCE command was used. Each pore/wall fraction was traced six times, three for the area calculation and three for the perimeter calculation. This way, an average reading could be taken to give greater accuracy.

The DELTA setting of .2 cm. was found to give the best combination of accuracy in measurement and speed in computation. The lower limit for area measurement of circular pores, for example, would be .004 cm . This represents 3% of the area of the 2 p.c.f foam and 1% for the 6 p.c.f. foam. Similarly, the smallest perimeter measurement possible was .04 cm., which was 2.5% of the total perimeter measured for the 2 p.c.f. foam and 1% for the 6 p.c.f. foam.

For any one picture, it was necessary to measure the total pore area and total wetted perimeter of all pores. The picture area and perimeter wre constant in each case (area = .068 cm , perimeter = 1.05 cm.). Porosity was then calculated as:

P = Void volume/ Bulk volume

= Total pore area/ Picture area

= Total pore area/ .068

This assumes that the flow through the foam takes place via channels of variable cross section and that the flow path length is equal to the sample length. This is consistent with assumptions used by Kozeny in his permeability model development.

Specific surface was calculated as:

S = Internal surface area/ Bulk volume

= Total wetted perimeter/ Picture area

= Total wetted perimeter/ .068

Tables 1 and 2 present these results.

2.6 Material testing

The interpretation of the results of the flow experiments required a knowledge of the mechanical properties of each polyurethane foam, e.g. tensile strength, ultimate elongation, and stress/deformation behavior. Since limited product data was available for both foams, it became necessary to conduct material testing to obtain the needed information.

An experiment was designed to measure the effect of compressive loading on small samples of 2 and 6 p.c.f. foam. The apparatus which was used is shown in fig. 10. A circular piece of 2 p.c.f. foam (10 cm. diam.) of length 1.25 cm. and a piece of 6 p.c.f. foam with the same diameter and length 2.54 cm. were used as test samples. Each piece of foam was placed between two rigid parallel plates. The bottom surface

was a 2.54 cm. thick piece of aluminum which was clamped onto a table top. A 1.25 cm. hole was drilled through the base, table top and the foam sample. The top plate was actually a piston made of .32 cm. thick sheet metal which had a .95 cm. aluminum rod screwed through the center of the plate. The piston rod was inserted through the hole and extended underneath the table. A bucket was attached to the end of the rod by means of three equally spaced wires. These provided stability for the system. The load was applied to the foam by adding water to the bucket. Since the base plate and piston were parallel at all times, the stress within the foam was evenly distributed. A dial indicator was clamped onto the base with the tip flush against the top plate. With this indicator, it was possible to measure small deformations of the foam to within .0013 cm.

The experimental procedure was then to pour a known volume, and hence weight, of water into the bucket. Stress was computed by dividing the weight of the water by the load application area. The change in length of the test sample was then read off of the dial indicator. Compression ratio was calculated as:

$$\lambda = \frac{L_o - \Delta L}{L_o}$$

Stress/compression ratio curves were plotted for each type of foam and are shown in figs. 11 and 12.

Both curves exhibit the same general behavior. There is an initial elastic region where deformation varies linearly with stress (labelled 1 on curves). The second

region (2) corresponds to a sudden relaxation of the foam. An infinitesimal increase in stress causes large deformation. This "plateau" region is more pronounced in the 2 p.c.f. foam. The final region (3) is marked by very large increases in stress with no noticeable further deformation.

All material testing was done on new foam samples which were previously undeformed. It became evident during the testing that hysteresis was present in the curves for both foams. As the foam is compressed and relaxed repeatedly, the stress/deformation curve shifts toward downward, i.e. less stress produces more deformation. This effect is well known (Ellas, Jones) and is referred to as conditioning. Since the material used in the flow experiments was new, the stress/deforamtion curve corresponding to new material was used.

CHAPTER 3

FLOW EXPERIMENTS

3.1 Flow apparatus

The apparatus used in all flow experiments was a simple closed-loop system consisting of a reservoir, test section with compressing piston, flow meter, sump and pump. (see fig. 13). The reservoir sat on an adjustable height stand which allowed the pressure head to be varied directly by raising or lowering the platform. A total head of 100 cm. was obtainable with this configuration. The outlet pipe was fitted with a hosecock which provided a continuous regulation of flow and allowed the flow rate to be set to the desired level. Because the flow rates were small, on the order of 6-60 ml/min, the head was maintained constant at each distinct flow setting while a was being taken.

The test section (fig. 14) was constructed of .625 cm. plexiglass. It consisted of two 11.5 cm. cylinders open at one end. Each cylinder had a 5 cm. width annular flange attached at the open end. The flanges had six equally spaced .31 cm. holes drilled through which enabled the two cylinder halves to be bolted together. A center plate of diameter 16.5 cm. was bolted betweenthe two halves. The plate had an 11.5 cm. hole in the center into which was inserted a .75 cm. long piece of stainless steel honeycomb material. This acted as both a flow staightener and a rigid porous base

plate on which the foam was attached. Each foam sample used was 11.5 cm. in diameter and 2.54 cm. long. The foam was bonded to the base plate using 3M 77 Spray Adhesive. Pressure taps were installed at the entrance and exit of the test section. A silicon oil filled manometer was used to measure the pressure drop across the foam.

External compression of the foam was supplied by a porous piston (see fig. 14). This device consisted of an 11.5 cm. diam. piece of metallic honeycomb mesh fitted into a .45 cm. plexiglass sleeve. The mesh was of the same type used for the center base plate. A tri-propeller 1.25 cm. plexiglass strut was used to attach the sleeve to a 1.25 cm. aluminum rod which extended outside the test section . The piston was held in place by an aluminum U-shaped frame (23.13 x 20.94 x 23.13 cm) which was bolted through the flanges and center plate of the test section. The outer end of the rod was threaded allowed the piston displacement to be controlled by rotating a knurled knob which fit onto the rod. Exact displacement was measured with a micrometer which was accurate to within .025 cm.

Dow Corning 200 silicon oil with a viscosity of 1 kg/m^3 was the fluid which was used in all experiments. This helped to maintain low Reynolds numbers (10^{-6}) .

3.2 Dimensional considerations

The dimensions of both the honeycomb and the foam became important considerations when trying to maintain one-dimensional flow. The honeycomb material used had

hexagonal shaped holes with a width of 1.8 mm. This was large compared with the hydraulic radius of each type of foam: .156 mm for the 2 p.c.f. foam and .09 mm. for the 6 p.c.f. foam. This gave an area ratio of at least ten to one and insured that the flow that entered the foam would not be obstructed and would be one dimensional. The base plate was modified to insure that the flow did not leak out through the perimeter of the foam. Leakage would cause the measured values of permeability to be higher than the true permeability. This was done by blocking a 2 cm. annulus on the outer edge of the honeycomb. The tortuosity of the foam (flow path length/ sample length) was assumed to be on the order of 1-1.5. If the flow was confined to a 7.5 cm diameter area then all flow paths would exit via the front face in the axial direction.

The test sample had a diameter/length ratio of three to one (7.5/2.54 cm.). This insured that no buckling of the foam would occur when the flow was compressive. Buckling would cause an uneven distribution of stress within the foam and would also allow flow leakage at the outer perimeter of the sample. The three to one diameter/length ratio also meant that derivatives in the y-direction would be small and so flow would be nearly one dimensional. speaking, the ratio should have been much smaller than one if the flow was to be truly one dimensional; but the y-component of the flow was assumed to be very small due to the straightening action of the honeycomb and therefore the assumption of one

dimensional flow would be valid even for this ratio.

The flow meter was a simple linear resistance type. It consisted of a 2.54 cm. O.D. plexiglass tube with 25 drinking straws contained inside. The pressure drop across this resistance was measured with another manometer and was used to calculate the flow rate of oil through the system. Calibration of the meter was done with a timer and glass beaker. The calibration curve is shown in fig 15. Least squares fit of the data gives:

$$q = .51\Delta p - .0124$$

where q is in l/sec * 10^4

Δp is in cm. H_2O

3.3 Flow experiments

The flow experiments conducted on each of the two foams were of three types:(see fig.16)

1.) Foam tethered upstream of flow, no external compression

2.) Foam tethered downstream of flow, flow-supplied compression

3.) Foam tethered upstream of flow, external compression supplied by porous piston

In the first experiment, pressure heads of 10-100 cm. were supplied in order of increasing magnitude in increments of 10 cm. At each head, 4-5 readings of pressure drop across the foam were taken corresponding to various flow rates. The process was repeated for a head of 100 cm. back down to 10 cm. to determine whether or not there was

any hysteresis in the flow curve, which could be produced by stress relaxation of the foam. The flow curves for each foam are shown in figs. 17 and 18.

The same procedure was used for the flow-induced compression experiments. However, the highly deformable nature of the polyurethane foams which were used required that adjustments be made in the experimental procedure. Compression of the foam generated internal stresses which relaxed over a period of time and approached some equilibrium value. Because of this, it was necessary to wait until steady state was reached before taking a reading. In order to determine the time scale of the relaxation process, a compressive pressure gradient of 90 cm. was suddenly imposed at time t=0 and measurements of pressure/flow were recorded at one minute intervals. The permeability of the foam was then calculated and plotted versus time. This was done for both foams . The results are shown in figs. 19 and 20. From these, it was determined that steady state was reached at 25 min. for the 2 p.c.f. foam and 20 min. for the 6 p.c.f. Pressure/ flow measurements could then be taken. For the 6 p.c.f. foam, it was impossible to obtain more than one reading at any particular head due to the minute magnitude of the flow. In fact, the flow rates were so small that they had to be measured by hand using a glass beaker and automatic timer. Figs. 21 and 22 show the results

for flow-induced compression on 2 p.c.f and 6 p.c.f. foam.

The final experiment performed involved the use of the porous piston described earlier to compress the foam. A non-dimensional compression ratio, , was defined in eq. 2.1 as:

$$\lambda = \frac{L_o - \Delta L}{L_o}$$

λ was varied from 1 to .3 for the 2 p.c.f. foam and from 1 to .55 for the 6 p.c.f. foam. The lower limit of .3 (and .55) was a restriction imposed by the fact that the compression was set by hand. It was impossible to go below that value without the use of external mechanical force.

The pressure head supplied for this case was kept low (15 cm.) so that no flow-induced distension of the foam occured. Any expansion of the foam would increase the flow rate and produce dsistorted values of permeability. Pressure/ flow readings were taken at each λ setting. Permeabilities were then calculated and plotted against λ . These are shown in figs 23-24 and will be discussed in the next chapter.

CHAPTER 4

DISCUSSION OF RESULTS

4.1 Prediction of permeability from foam geometry

Attempts to establish an empirical relationship between permeability and various dynamical properties of porous media have been sought for at least forty-five years. The simplest correlation would be the one between porosity and permeability. Mavis and Wilsey (1937), Jacob (1946), and others have explored this line of thought and have all claimed to have found permeability (K) to be directly proportional to porosity, i.e.:

$$k = p^n \qquad \text{Eq. 4.1}$$

where n= 5 or 6 (Mavis)

= undetermined (Buche 1937)

However, such a simple correlation is not reasonable and can't really exist. It is possible for two foams to have the same porosity and have different permeabilities. In fact, all of the above mentioned theories do contain other factors such as pore diameter which need to be defined and adjusted in order to make the correlation fit. Determination of porosity alone is not sufficient to calculate the permeability of a porous medium.

A second possibility is to relate the structure of porous media to the permeability. This, in effect, requires that the pore size distribution be known. It is not a simple

process to obtain this information and the results of such experiments have been unsuccessful (Nelson and Baver, O'Neal).

The most successful models to date couple empirical and theoretical considerations to determine permeability of porous media. The theory involves the analysis of the microscopic flow through porous media. The earliest investigation using this rationale was performed by Kozeny in 1927. Kozeny's work is still widely accepted as an explanation for the permeability as conditioned by the geometrical properties of a porous medium. Kozeny represents the porous medium as an assemblage of channels of various cross sections, but of a definite length. The Navier-Stokes equations are solved simultaneously for all channels passing through a cross section normal to the flow in the porous medium. The assumption is made that there is no tangential component of the fluid velocity. The theory is not presented here, but may be seen in detail in Scheidegger. Kozeny's theory results in a solution for the flow through a porous medium.

$$q = \frac{-cP^3}{\mu S^2} \text{ grad } p \qquad \text{Eq. 4.2}$$

Comparing this with Darcy's law, the permeability is found to be:

$$k = cP^3/S^2 \qquad \text{Eq. 4.3}$$

The variable c, known as the Kozeny constant, is a bone of contention among those who have tried to experimentally verify Kozeny's theory. In Kozeny's own

experimentally verify Kozeny's theory. In Kozeny's own development, this constant is a function of channel geometry and varies only slightly. For a circular channel c = .5, for a square c = .5619, and for an equilateral triangle c = .5974. Carman (1937) found that c = .2 gives the best agreement with experimental data.

The question then arises as to the correct value of c to use in evaluating the Kozeny permeability. Strictly speaking, the porous media being examined are not a collection of channels. They appear more as a series of intertwine fibers. Certainly, this is the appearance of the trabecular meshwork; and if any relevant conclusions are to be drawn from photographs of the meshwork then it is necessary to apply an accurate model.

The answer to the question may be found in the analysis performed by Happel (1959) on viscous flow relative to an array of cylinders. Happel uses two concentric cylinders as a model for fluid moving through an assemblage of cylinders . The Navier-Stokes equation is solved for both cases with the appropriate boundary conditions. The expressions obtained for the flow rate are compared to Darcy's equation and values of the Kozeny constant are obtained for each flow case. In the case of a random configuration of cylinders, a weighted average of 2/3 the value for perpendicular flow and 1/3 the value for parallel flow is used to obtain a final expression for the constant c:

$$k = \frac{1}{c} = \frac{4P}{3(1-P)\ \ln(1/1-P)\ \frac{1-(1-P)}{1+(1-P)}}$$

$$+ \frac{2P}{3(1-P)\ 2\ \ln(1/1-P) - 3 + 4(1-P) - (1-P)}$$

Davies studied beds of fibers which were packed in a uniform manner to give high porosities in a range of .7-.994. From this investigation, he obtained an empirical solution from which the Kozeny constant can be computed. His findings support Happel's calculations for c, especially at high porosities. So it seems reasonable to use Happel's work in conjunction with the Kozeny equation in order to calcualte the permeability of porous media based on its geometric properties.

4.2 Calculation of permeability

As previously stated, one of the goals of these experiments was to determine the undeformed permeability of the porous media by two distinct methods:

1.) Optical experiments using Kozeny's relationship

2.) Flow experiments using Darcy's law

These calculations will now be presented.

4.2.1 Kozeny calculations

In the last chapter, methods were described for obtaining measurements of all the pertinent parameters. These are:

1.) Porosity

2.) Specific surface

Knowledge of the sample porosity allows us to determine the constant c using eq. 4.4. Finally, the permeability is

computed using eq. 4.3. Results for the 2 p.c.f. and 6 p.c.f. foams are shown in Tables 3 and 4 respectively.

4.2.2 Darcy's law

The permeability of the polyurethane foam was determined for each of the three flow regimes from flow data using the one-dimensional Darcy relationship:

$$k = q L_o/\Delta p \qquad \text{Eq. 4.5}$$

where q is flow rate/unit area

$(l/sec*10^4)$

L_o is sample length

Flow rates and pressure drops had been measured and viscosity was known to be 1 kg/m^3. Values for permeability were plotted versus pressure drop for extension and compression and are shown in figs. 25-28. Fig. 23-24 show the result for the externally compressed flow case. Undeformed permeability corresponds to $\lambda = 1.0$ in the externally compressed flow and to near zero flow rates in the flow expansion and compression case. The permeability for the 2 p.c.f. foam is 4.0-4.2, while that of the 6 p.c.f. foam is 1.8-2. As expected, these values are the same for the three different sets of experiments.

This is in good agreement with the values obtained for permeability from photomicrograph analysis (see table 3,4) Flow-measured permeability for the 2 p.c.f foam falls near the mean value of 4.12 and that of 1.74 for the 6 p.c.f. foam. The fact that the standard deviation of values for permeability calculated from photomicrographs is high

could be a product of the technique used to set the foam and photograph it. The presence of the thin film coating observed in the SEM's of the foam did affect the total removal of air from the samples, particualarly the 6 p.c.f. foam. This in turn could affect the clarity of the pictures and the number of suitable samples available for analysis. The discrepancies could possibly be reduced by improving the method of obtaining photomicrographs.

Another possibility for the error could be the remainder of air in the foam sample used in the flow experiments. The presence of air would increase the flow resistance and distort the measured value of permeability.

The use of the Kozeny relationship with Happel's value for the Kozeny constant does appear to be justified, however. It does give a quantitative measure of the permeability, and hence resistance, of the porous media used.

4.3 Effect of expansive flow on permeability

The effect of increasing flow on the permeability of the upstream-tethered foam was the same for both the 2 and 6 p.c.f. foam. Namely, an increase in the pressure produced an increase in the permeability. The increase is fairly linear with pressure.

The relative change in permeabilities did vary between the two foams. Expressed in terms of fractional change in permeability/ fractional change in pressure, this can be written as:

fractional k= .38 for the 2 p.c.f. foam

fractional p= .61 for the 6 p.c.f. foam

This indicates that the 6 p.c.f. foam requires a smaller fractional increase in pressure than the 2 p.c.f. foam to produce the same fractional increase in permeability.

The effect of the pressure seems to be to open up the pores and to elongate the foam. It would appear that the 2 p.c.f. foam has the potential to expand more and hence produce larger increases in permeability. The total % change in permeability of the 2 p.c.f. foam was 123 % as compared to 91.8 % for the 6 p.c.f. foam. This difference can be explained by comparing the tensile strength and ultimate elongation for both foams. The tensile strength of the 2 p.c.f foam is 65 kpa. compared to 107 kpa. for the 6 p.c.f. foam. Ultimate elongations are 200% and 160% respectively. Unfortunately, the elongation was not measured in these experiments. If this information had been available it would be easier to assess the effects of increased pressure on permeability.

4.4 Effect of compression on permeability

The most interesting results are those of the compressive flow experiments: both flow-induced and external. Compressive flow through porous media produces an overall reduction in permeability. The amount of reduction and its manifestation varies between the 2 and 6 p.c.f. foam.

The discussion of these results will be presented

as follows:

1.) 6 p.c.f. foam

2.) 2 p.c.f. foam

3.) comparison with Beaver's work

4.4.1 6 p.c.f. foam

The externally compressed 6 p.c.f. foam shows a strong relationship between permeability and compression ratio. A rapid decrease in permeability occurs with a decrease in λ . In the region of λ = 1-.9, the permeability drops off dramatically- from the undeformed value of 1.91 to one of .138. The rate of decrease in k levels off at a value of λ of about .95. The permeability decreases slightly with further decreases in λ until the experimental limit of λ = .55 is reached. As mentioned previously, it was impossible to compress the foam manually beyond that point in the current apparatus. This can easily be explained by referring to the curve for 6 p.c.f. foam. λ of .55 corresponds to the point where the stress increases almost asymptotically. This would appear to be a region of near collapse of the foam, but with a considerable volume of trapped fluid. It is possible that the thin film coating that was seen in the S.E.M. photographs of the foam actually closed off some of the pores and trapped air inside. This would then make it impossible to totally compress the foam.

In the flow-induced compression, it seemed peculiar that the permeability had an initial value 35 X lower than the undeformed value, even at low pressures. However, the σ/λ

and k/λ curves provided some insight into this situation. The permeability established itself at .053 and fell linearly with pressure drop to a value of .032. This range of permeability would correspond to a compression ratio of .8 on the σ/λ curve, which translates into a stress of about 5.9 kpa. According to eq. 1.1

$$\frac{d\sigma}{dx} = \frac{dp}{dx}$$

This can be integrated to give

$$\sigma_{u.s.} - \sigma_{d.s.} = -(p_{u.s.} - p_{d.s.})$$

at the exposed face of the foam

$$p = p_o$$

In order to satisfy the requirements that

$$\frac{F}{A} = \sigma + p$$

and

$$\frac{d}{dx}(F/A) = 0$$

the upstream stress must be 0. This gives the result that

$$\sigma_{d.s.} = \Delta p$$

This says that the maximum stress produced within the foam is equivalent to the pressure drop established in the flow and that the effect of this stress will be concentrated at the tethered end of the foam. From this analysis, we would expect the pressure drop across the foam in this case to be 59 cm. H20. Referring to fig., at k = .044, Δp equals 60.5 cm.

As one would expect, therefore, flow acts to effectively decrease the compression ratio of the foam in

this series of experiments. A higher pressure produces a lower compression ratio and hence a lower permeability and vice versa.

4.4.2 2 p.c.f. foam

The results for externally compressed 2 p.c.f. foam differ from those of the 6 p.c.f. foam. There is no dramatic drop in permeability. Rather, the permeability decreases uniformly with a decrease in λ. No explanation is obvious for this behavior. One possibility is illustrated in fig. 29. Pores are represented as the junctions of spherical inclusions which make up the foam. As the compression ratio increases, the pores begin to close off. The pores in the 6 p.c.f. foam are smaller than those in the 2 p.c.f. foam and collapse at a higher compression ratio, thereby producing the large decrease in permeability seen at high λ. The pores in the 2 p.c.f. foam close more slowly and hence the decrease in permeability is less marked than that of the 6 p.c.f. foam. No definite conclusion can be reached about the exact nature of the decrease in permeability of the 2 p.c.f. foam, only that it does decrease with a decrease in λ.

The flow induced compression of 2 p.c.f. foam also produced results which were puzzling. Since the permeability is a function of compression ratio, which is the case for the 6 p.c.f foam, then one would expect a decrease in the permeability with a decrease in λ. This is not the case, however. The permeability does not significantly depart from its undeformed value of 4.2. It remained at a constant value

of about 3.75. One possible explanation for this behavior follows from the analysis presented in the previous section. It was seen that the stress at the downstream end of the foam was equal to the total pressure drop across the foam. This could produce a decrease in the permeability for this downstream region. The rest of the foam feels less compression and its permeability will remain close to the undeformed value. The overall permeability for the foam sample would therefore not be significantly reduced. This would be better shown if the experiments were extended to incude the region where pressure drop across the foam exceeds 30 cm. This is equivalent to a stress of 3 kpa, which corresponds to the point on the σ/λ curve where the compression ratio decreases dramatically with a small increase in stress. At this point, one would expect to see a very dramatic decrease in permeability, similar to the kind observed in the 6 p.c.f. foam. If this did not occur, then the explanation put forth would be plausible.

4.4.3 Comparison to Beavers and coworkers work

At this point, it would be useful to compare the results obtained in both the 2 p.c.f. and 6 p.c.f. compression flow case to similar work done by Beavers et al. A brief digression is necessary to place their work in perspective.

Beavers and colleagues defined a Reynolds number based on permeability as an effective way to differentiate between Darcy and non-Darcy flow:

$$RE = \frac{\rho u \sqrt{k}}{\mu}$$

Using this definition it was possible to calculate Re # for both foams in all three flow regimes. Results are shown in Table 5. Beavers noted significant departure from Darcy flow at Re = 1. Re # in the present experiments were on the order of 10^{-5} to 10^{-6}. This is clearly Darcy flow. The experiments conducted by Beavers et al dealt specifically with non-Darcy flow. However, the implications of their work apply to both high and low Re # flow.

The material curves for the foams used by Beavers et al are shown in fig. 29. Foam A has a density of 70.5 kg/m while foam B has a density of 25.9 kg/m . The density ratio for foam A and B is 3:1, which is the same as that of the 6 and 2 p.c.f. foams. The curves for those foams are shown again in fig. 30. Comparison of the two figures shows that the two foam types are similar but not exactly the same. The elastic limit of the 2 p.c.f. foam occurs at a slightly higher value of stress than the Beavers et al foam B. Also, the magnitude of the stress in the 6 p.c.f. foam is greater than that of the foam type A. However, the curves are similar enough to allow qualitative comparisons to be made between the two studies.

Beavers and coworkers' results for permeability as a function of compression ratio are shown in fig. 31. Figs. 32-33 show 1/k plotted versus deformation for both foams used in the present experiments. All three curves show the same relative increase in 1/k with decrease in λ .

A second comparison can be made between flow induced compression results from Beavers et al (fig. 34) and the results that appear in figs. 21 and 22. Beavers and coworkers' data shows a fairly linear relationship between $\dot{m}$ and Δp in case B. This is similar to the curve for the 2 p.c.f. foam used in the present experiments. The flow curve for material A exhibits more of a plateau at high Δp, which is comparable to the results obtained for the 6 p.c.f foam.

From these comparisons it would be reasonable to say that the presnt experiments do qualitatively agree with previous work conducted by Beavers et al.

4.5 Relevance of the study to the trabecular meshwork

The objective of this study with regards to the eye was to develop and demonstrate a general method which allows the flow properties of the trabecular meshwork to be inferred from photomicrographs. This has been proven to be valid using the Kozeny and Happel analysis. Useful information on trabecular meshwork geometry, i.e. porosity and specific surface, can be garnered with the photographic analysis described in section 2.3. The quantitative measurement of resistance can not be directly obtained with these results. The use of Happel's constant is not valid for porosities below .5, which is significantly higher than the porosity of the meshwork. Within this range, Happel's constant varies from 4.8 at a porosity of .5 to 28.8 at a porosity of .99. Below a porosity of .5, the Kozeny constant is higher than the Happel constant and therefore using

Happel's constant would give inaccurate results. An appropriate value of c would be needed to give a true quantitative measure of resistance.

One observation may be brought forth regarding the flow of aqueous humor through the meshwork. The analysis performed in section 4.2 would seem to indicate that the full effect of the pressure drop across the meshwork would be felt in the endothelial region, which is where the porosity is smallest. This would make it entirely possible for a large decrease in the permeability of this region to be experienced. Whether or not it would be significant enough to produce the large resistance seen in glaucomatous eyes is unknown.

The next step in the analysis of flow through the meshwork would be to develop a model similar to Beavers et al which would predict q vs. Δp . This would use the results of this study and would also incorporate more of the true physiological characteristics of the meshwork.

CHAPTER 5

CONCLUSIONS

The goals of these experiments were outlined in chapter 2 as:

1.) Perform a complete set of experiments

a) with little or no deformation

b) with external compression

c) with flow-induced extension and compression

2.) Develop a technique of determining permeability from photomicrographs

Both goals have been reasonably achieved.The permeability measurements obtained through flow experiments and computed using Darcy's law are in good agreement with the predictions based on optical measurements using Kozeny's and Happels work. The model works well with the highly porous media used in these experiments. Any application to the trabecular meshwork would have to be qualitative rather than quantitative due to the discrepancy in porosities which makes Happel's constant unusuable. The general model is sound, however.

The effect of extension and compression produced some results that were in keeping with previous investigations of similar problems. Extension flow produced an increase in the permeability of both foams. External

compression of the foam produced the result that permeability decreased with decrease in compression ratio. The effect was more pronounced in the 6 p.c.f foam than in the 2 p.c.f. foam. Flow-induced compression resulted in a similar decrease in permeability with increase in pressure drop. This leads to the conclusion that permeability is a strong function of compression ratio. Overall, the results compare favorably with recent work done by Beavers et al.

This study is presented as the first step in the development of a complete model to describe the fluid flow through a compressible medium with specific applications to the trabecular meshwork. Such a model does not exist as of yet. This makes it difficult to fully assess the results of these experiments. Yet, these results provide a good test for any future analytical models which are developed.

Future work would most likely be directed toward:

1.) Predicting the change in permeability with deformation

2.) Developing a complete flow model which would predict flow rate vs. pressure drop

REFERENCES

Battaglioli, J.L., "The Role of Vessel Collapse on the Flow of Aqueous Humor", Master's Thesis, Department of Mechanical Engineering, M.I.T., June 1981.

Baver, L.D., Soil Physics, Wiley, New York, 3rd ed., 1956.

Bear, J., Zaaslavsky, D., Irmay, S., "Physical Principles of Water Percolation and Seepage: Arid Zone Research",XXIX UNESCO Paris 1968.

Biot, M.A., "General Theory of Three-Dimensional Consolidation",J of Appl. Phys., Vol. 12, 1941, pp. 155-164.

Buche, W., 1937 Z Ver deuts Ing., Beih. Verf ahrenstech, 1937, p 155.

Chaudry, H.A., et al, "Scanning Electron Microscopy of Trabeculotomy Specimens in Open-Angle Glaucoma",Amer. J. of Opth.(1979) 88, pp. 78-92.

Dickey, G.D., Filtration, Reinhold, New York, 1961.

Dullien, "Determination of the Structure of Porous Media",Indus. and Eng. Chem.(1970) 62, pp. 25-53.

Elias, T.C., "Investigation of the Compression Response of Ideal Unbonded Fibrous Structures",Tech. Assoc. of the Pulp and Paper Indus., Vol 50, #3, 1967,

pp. 125-132.

Ergun, S., "Fluid Flow through Packed Columns", Chem. Eng. Prog., Vol. 48, 1952, p 89.

Grierson, I., Lee, W.R., "The Fine Structure of the Trabecular Meshwork at Graded Levels of Intraocular Pressure: (1) Pressure Effects Within the Near-Physiological Range (8-30 mm. Hg.), Expt1. Eye Res. (1975) 20, pp 505-521.

Happel, J., "Viscous Flow Relative to Arrays of Cylinders", AICHE J., 1959, Vol. 5, #2, p 174-177.

Harris, C.C., "Flow through Porous Media. Examination of the Immobile Fluid Model", Powder Technology (1977) 17, pp 235-252.

Hedbys, Mishima, Expt1. Eye Res. (1962) 1, p 262.

Henderson, Trans. Opthal. Soc. U.K. (1908) 28, p 47.

Johnson, M., "The Role of Schlemm's Canal in Aqueous Outflow form the Human Eye", Master's Thesis, Department of Mechanical Engineering, M.I.T., June 1981.

Jacob, C.E., 1946 Trans. Amer. Geophys. 27, p 245.

Muscat, M., Physical Principles of Oil Production, Mc-Graw Hill, New York, 1949.

Nelson, W.R., Baver, L.D., 1940 Proc. Soil Sci. Soc. Amer. 5, p 69.

O'Neal, A.M., 1949 Soil Sci. 67, p 403 .

Preston, B., Davies, M., Ogston, A., Biochem. J. (1965) 95, p 445.

Pryor, E.J., Mineral Processing, Elsever, Amsterdam, 3rd ed., 1965.

Scheidegger, A.E., The Physics of Flow through Porous Media, Univ. of Toronto Press, Toronto, Canada, 3rd ed. 1974, pp 137-140.

Sheffield, R., Metzner, A., "Flows of Non-Linear Fuids through Porous Media", AICHE J., Vol. 22, #4, 1976, p 736.

Terzaghi, K.,Theoretical Soil Mechanics, Wiley, New York, 1961.

Tripathi, R.C., Comparative Physiology and Anatomy of the Aqueous Outflow Pathway, Chp.3 inThe Eye, Vol. 5: Comparative Physiology, Ed. H. Davson, Academic Press, London and New York, pp 163-241.

Welderhielm, C.A., Fox, J.R., Lee, D.R., "Ground Substance Mucopolysaccharides and Plasma Proteins: Their Role in Capillary Water Balance"Amer. J. of Phys., Apr. 1976, pp. 1121-1125.

TABLE 1

POROSITY AND SPECIFIC SURFACE MEASUREMENTS

FOR 2 P.C.F. FOAM

Photograph	Porosity	Specific Surface (1/M)
1	.919	4732
2	.926	4613
3	.928	4667
4	.932	4624
5	.950	4583
6	.934	4757
7	.952	4226
8	.954	4230
9	.957	4301
10	.958	4243

TABLE 2

POROSITY AND SPECIFIC SURFACE MEASUREMENTS

FOR 6 P.C.F. FOAM

Photograph	Porosity	Specific Surface (1/M)
1	.848	8669
2	.849	8480
3	.854	8474
4	.856	8526
5	.860	8286
6	.861	8451
7	.864	8755
8	.865	8485
9	.868	7871
10	.873	7735

TABLE 3

CONSTANT (c) AND PERMEABILITY MEASUREMENTS

FOR 2 P.C.F FOAM

Photo.	Porosity	Constant (c)	Permeability
1	.919	.128	4.436
2	.926	.119	4.389
3	.928	.116	4.256
4	.932	.112	4.240
5	.934	.109	3.923
6	.950	.089	3.632
7	.952	.086	4.158
8	.954	.083	4.034
9	.957	.079	3.742
10	.958	.078	3.808

Mean value:4.06

Std. Dev.:.297

TABLE 4

CONSTANT (c) AND PERMEABILITY MEASUREMENTS

FOR 6 P.C.F. FOAM

Photo.	Porosity	Constant (c)	Permeability
1	.848	.202	1.639
2	.849	.202	1.719
3	.854	.196	1.700
4	.856	.194	1.7674
5	.860	.190	1.760
6	.861	.189	1.689
7	.864	.186	1.565
8	.865	.185	1.663
9	.868	.182	1.921
10	.873	.177	1.968

Mean value: 1.74

Std. dev.:.124

TABLE 5

RE # FOR FLOW EXPERIMENTS

Foam type	Experiment	RE # (*10E6)
2 p.c.f.	Extension	3.144-44.24
6 p.c.f.	Extension	2.718-20.95
2 p.c.f.	Compression	5.519-23.17
6 p.c.f.	Compression	.0082-.0472

LIST OF FIGURES

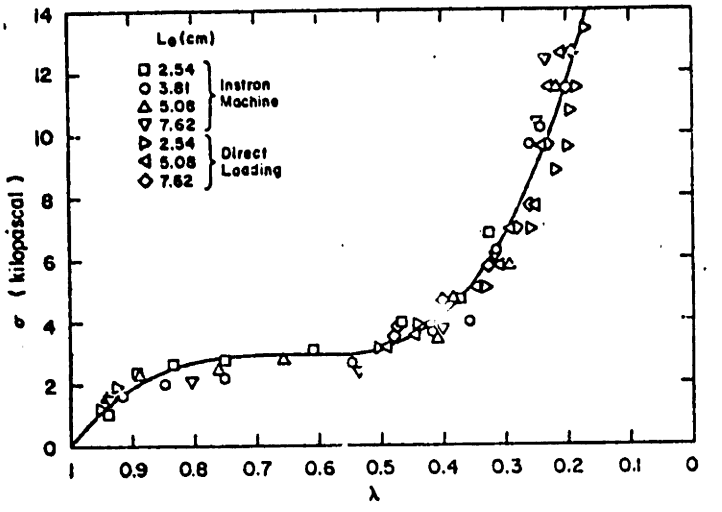

Fig. 2 Relationship between stress and compression ratio for polyurethane; the line is the empirical result given by equation (13)

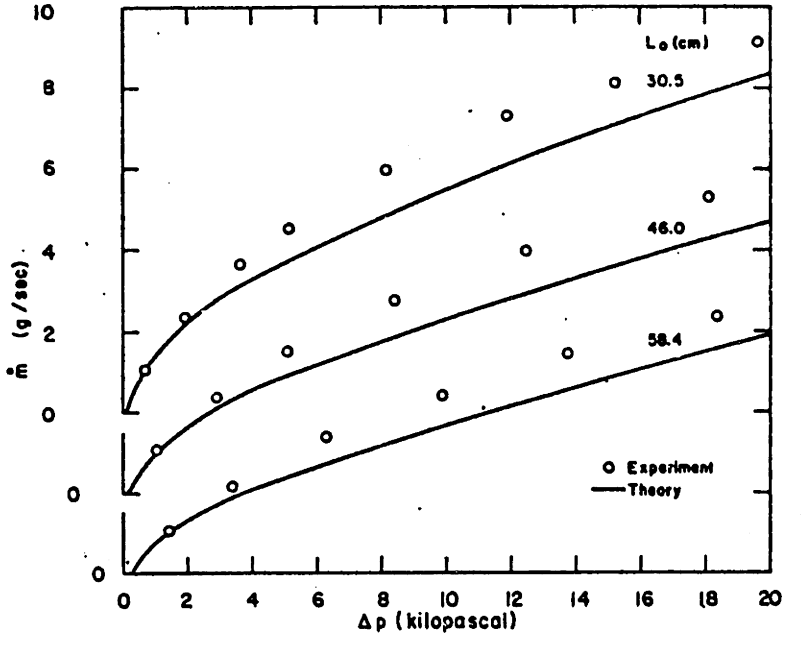

Fig. 7 Comparison between measured and predicted mass flow rates through three polyurethane specimens as functions of the applied pressure difference across the material

Figure 1

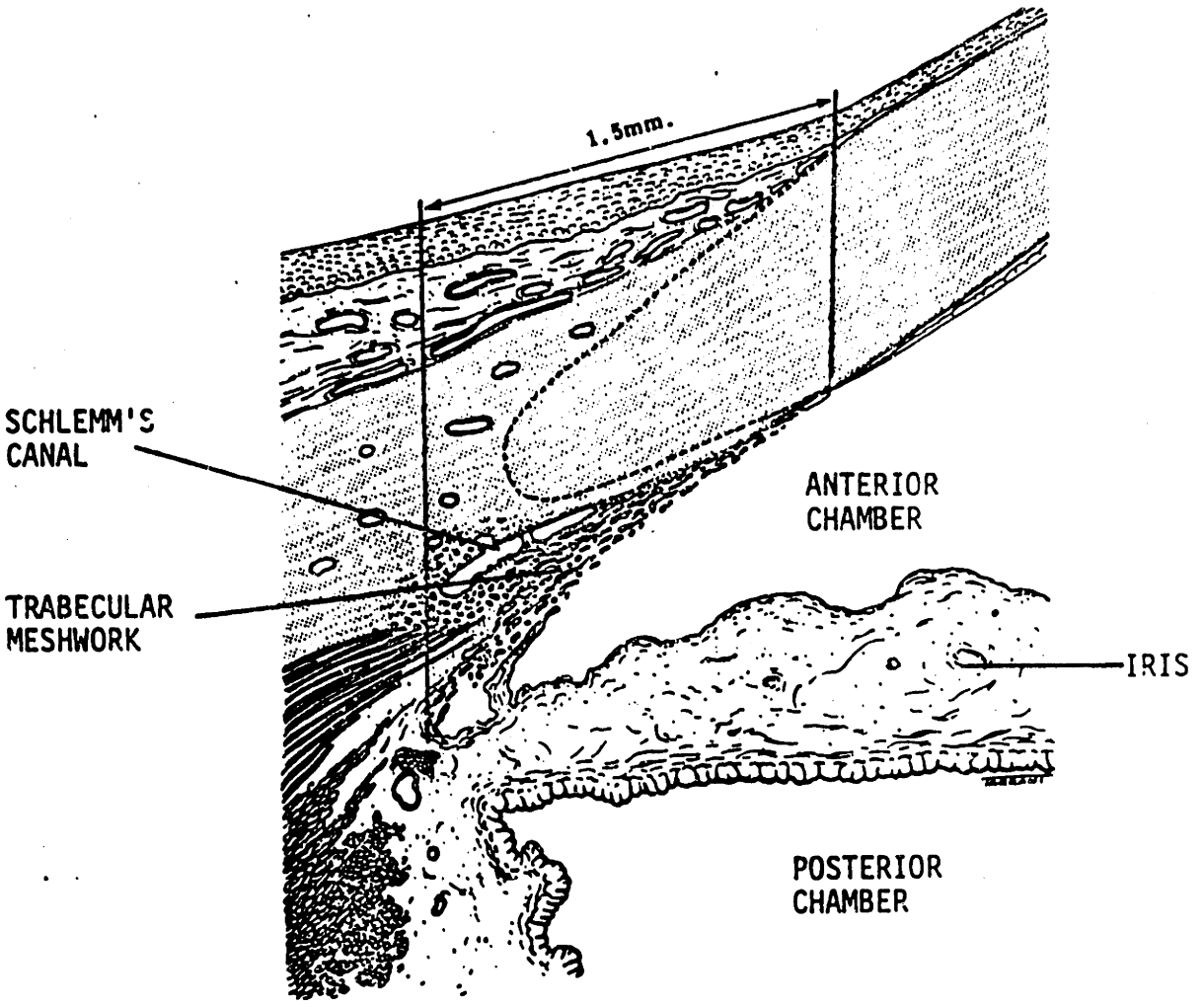
1.5mm.
SCHLEMM'S CANAL
TRABECULAR MESHWORK
ANTERIOR CHAMBER
IRIS
POSTERIOR CHAMBER

Figure 2

Figure 3

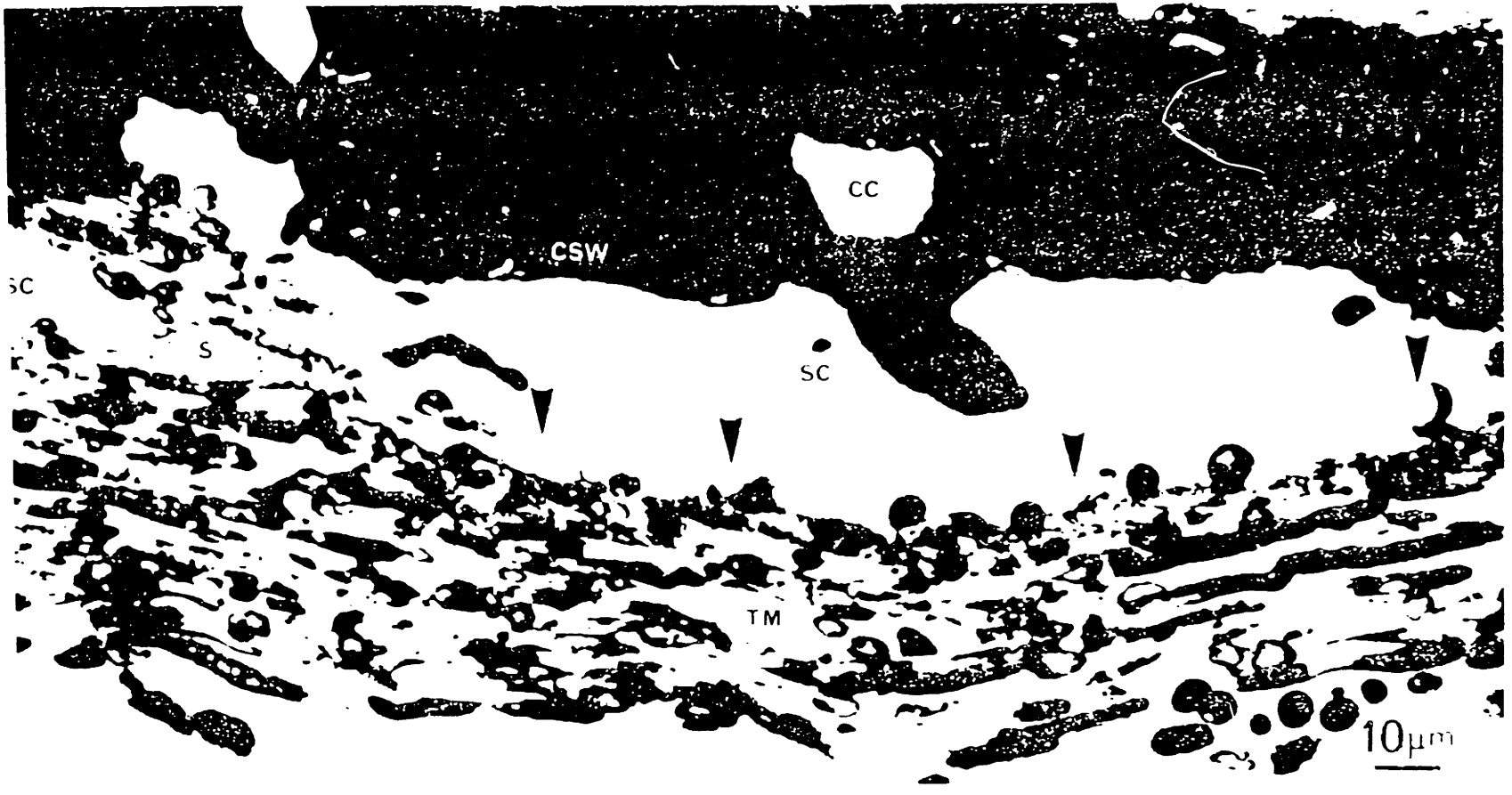

Figure 3

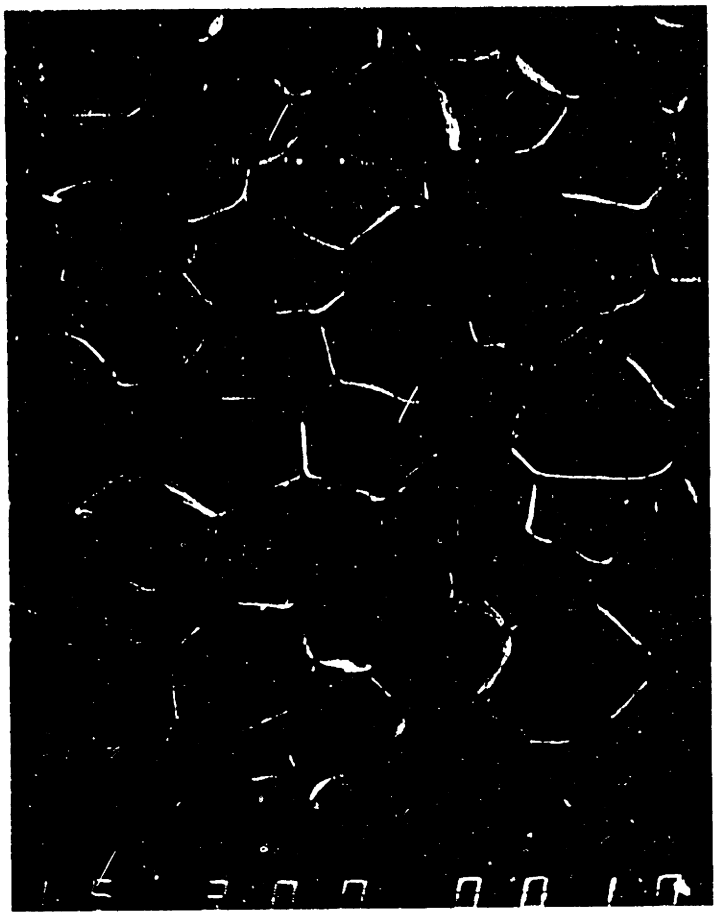

Figure 4

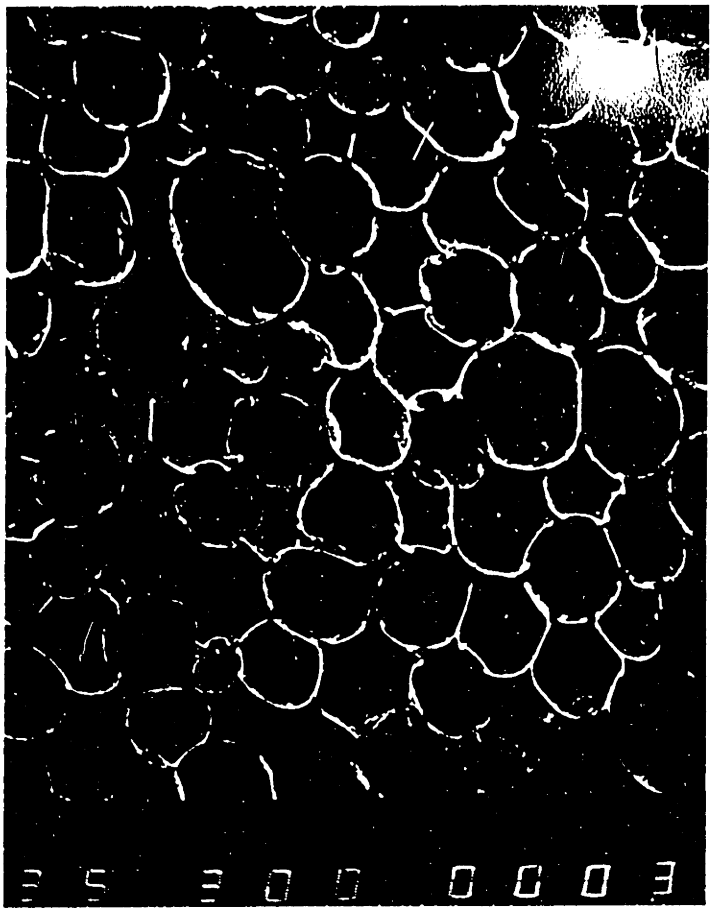

Figure 5

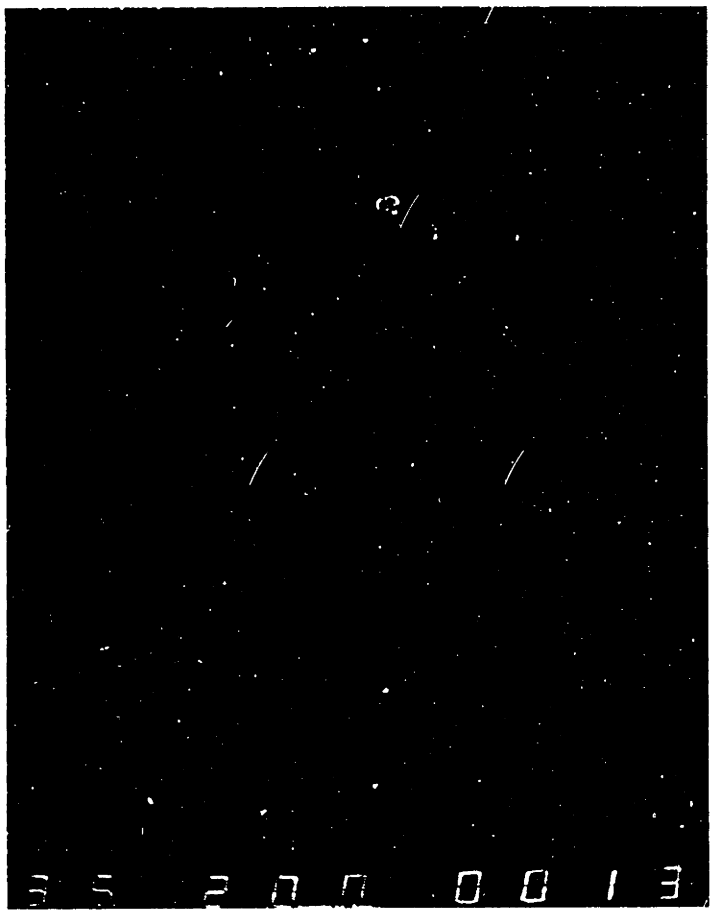

Figure 6

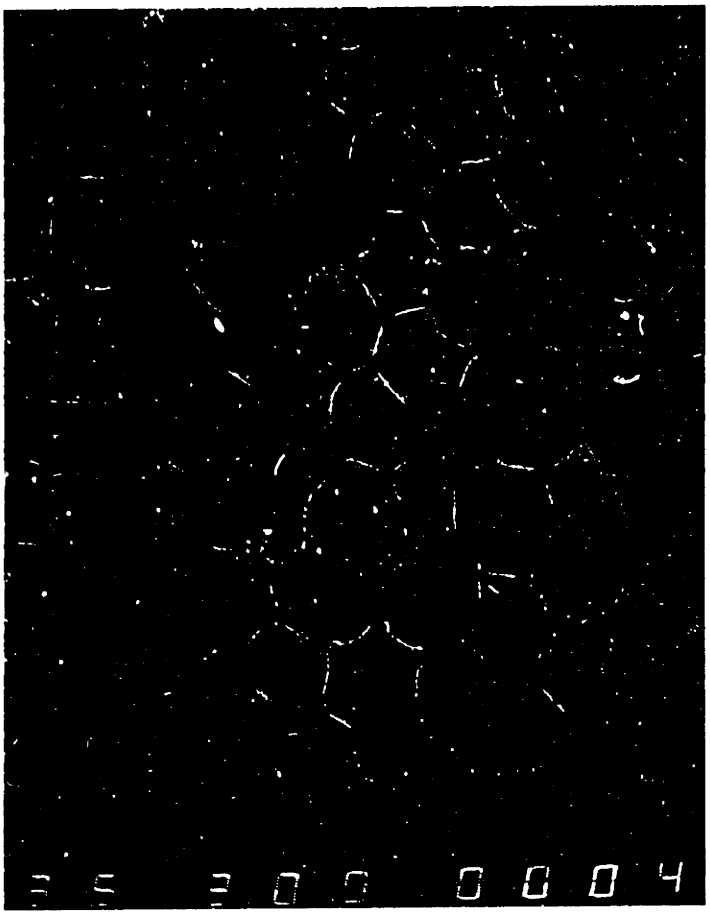

Figure 7

Figure 8

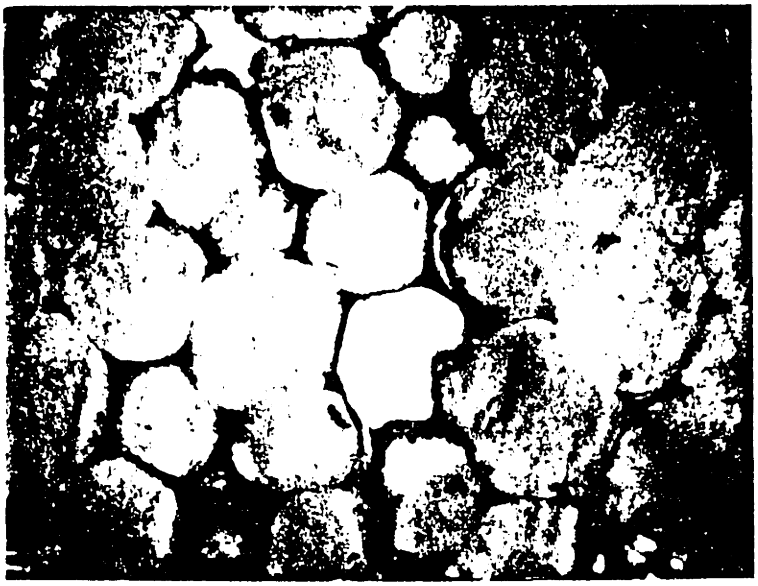

Figure 9

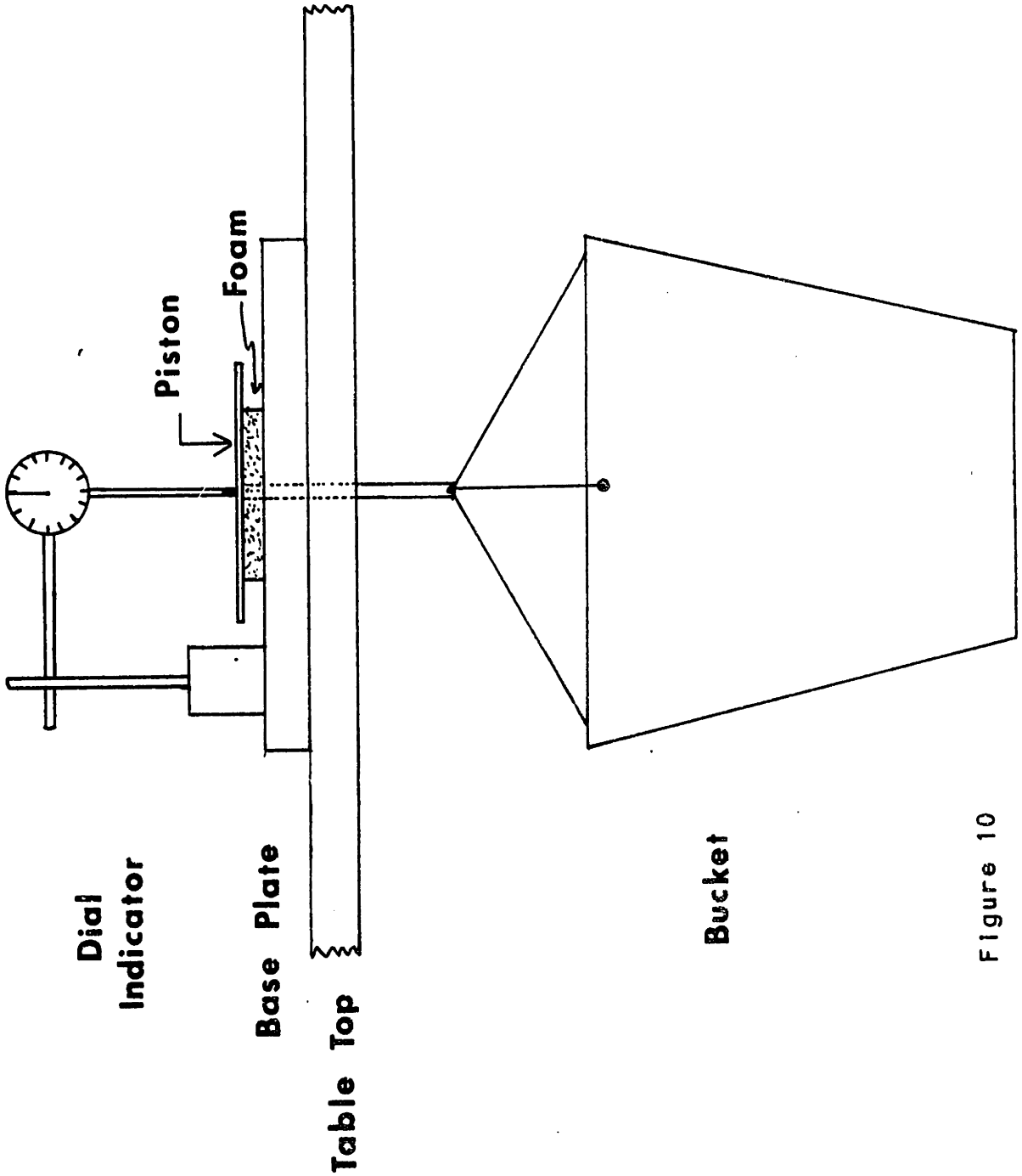

Figure 10

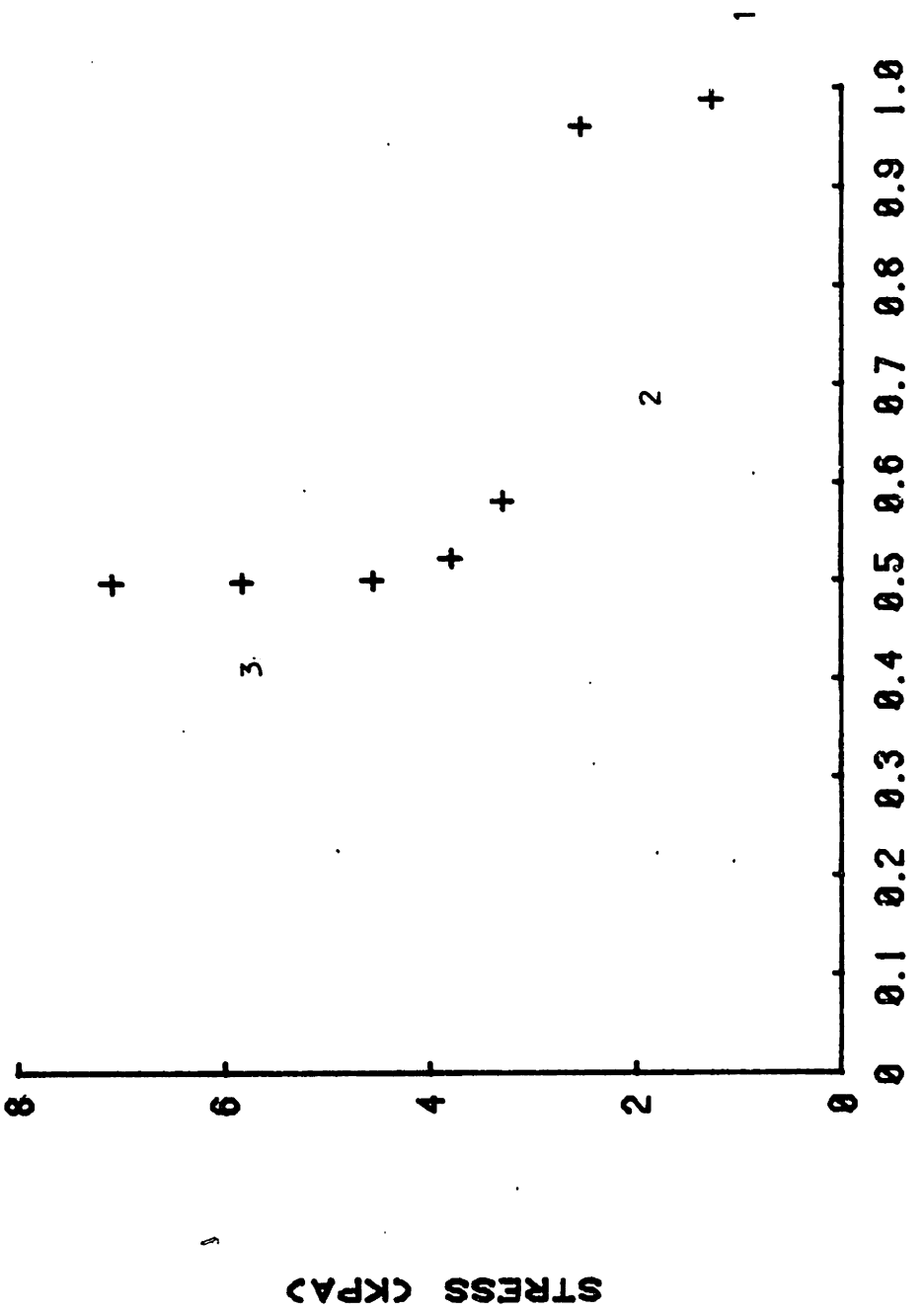
STRESS (KPA)
0
2
4
6
8
0 0.1 0.2 0.3 0.4 0.5 0.6 0.7 0.8 0.9 1.0
COMPRESSION RATIO
1
2
3

Figure 11

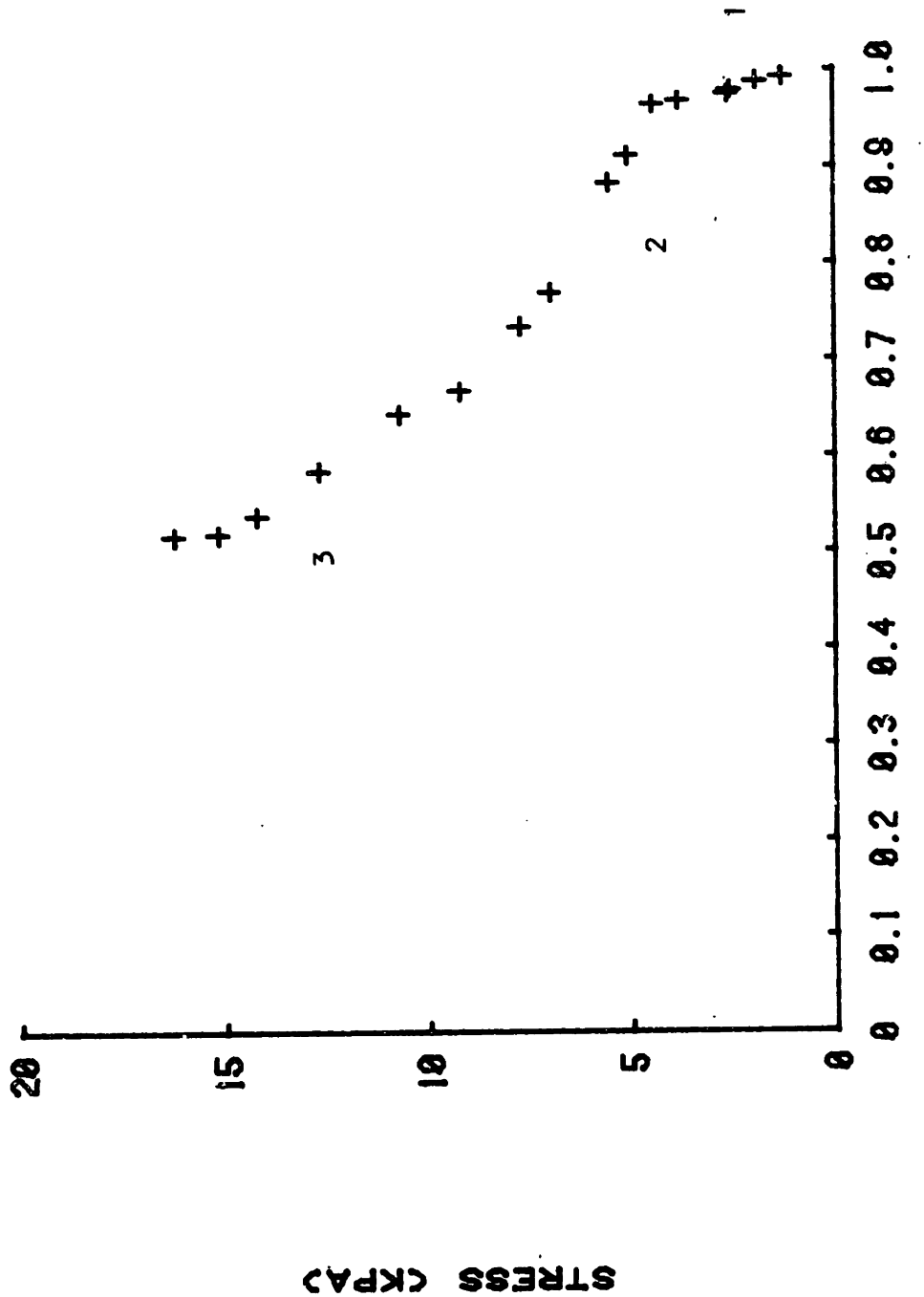
STRESS (KPA)
20
15
10
5
0
0 0.1 0.2 0.3 0.4 0.5 0.6 0.7 0.8 0.9 1.0
COMPRESSION RATIO
1
2
3

Figure 12

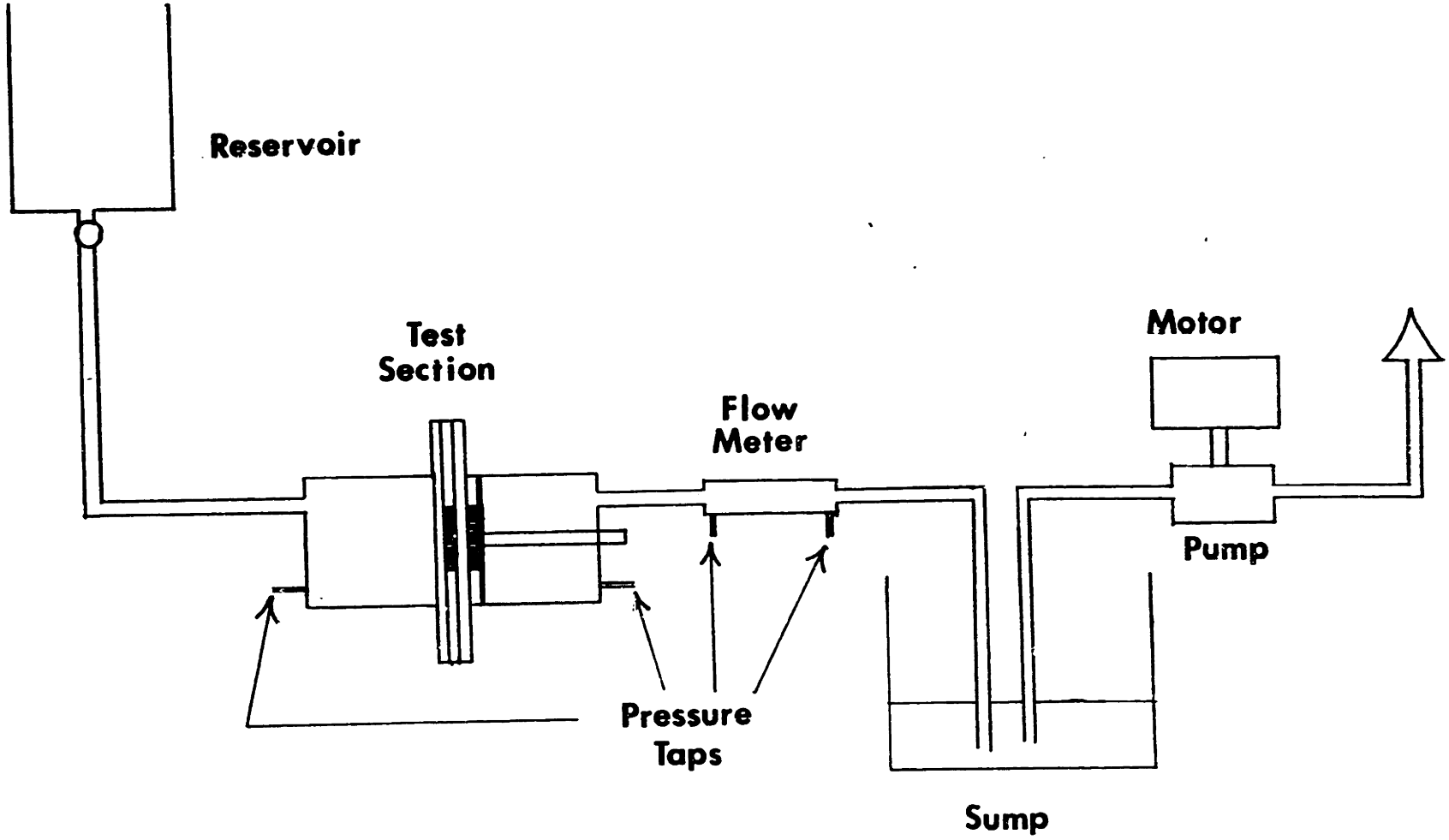
Reservoir
Test
Section
Flow
Meter
Motor
Pump
Pressure
Taps
Sump

Figure 13

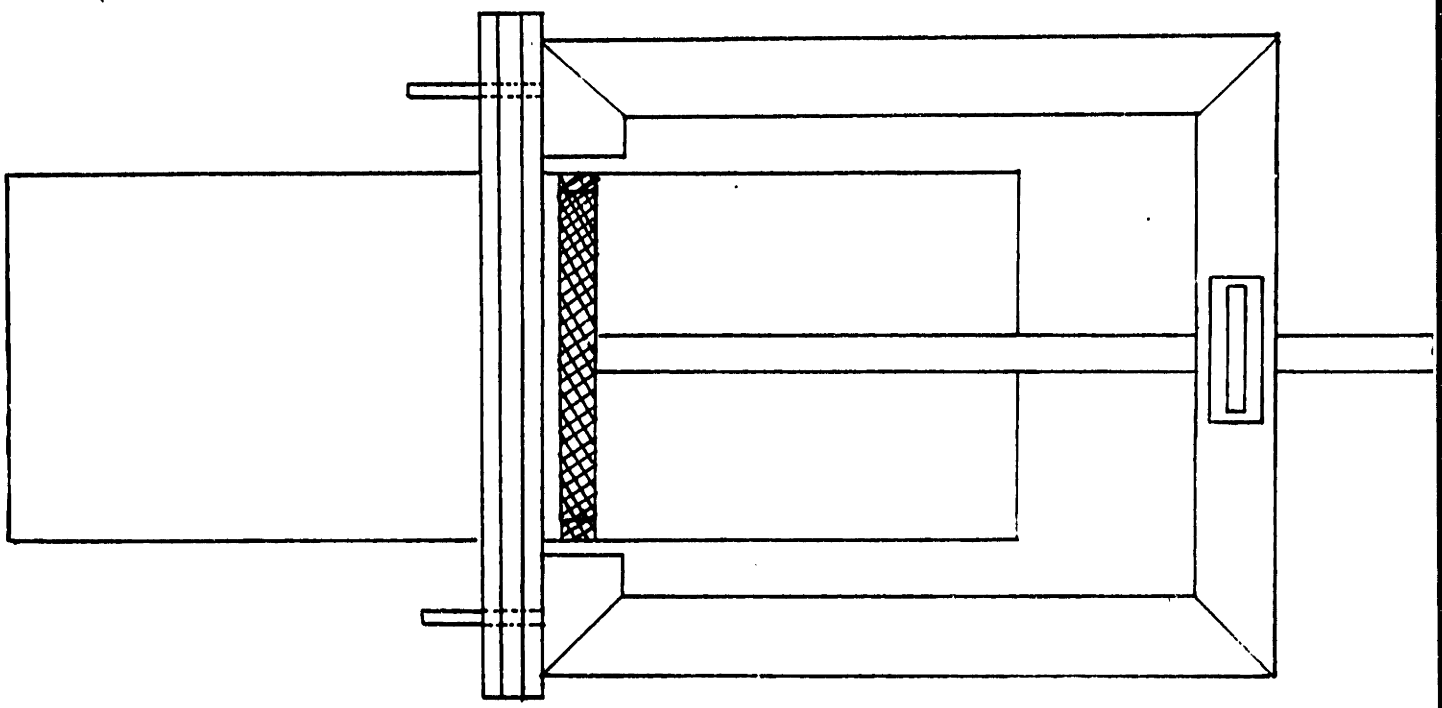

TOP VIEW

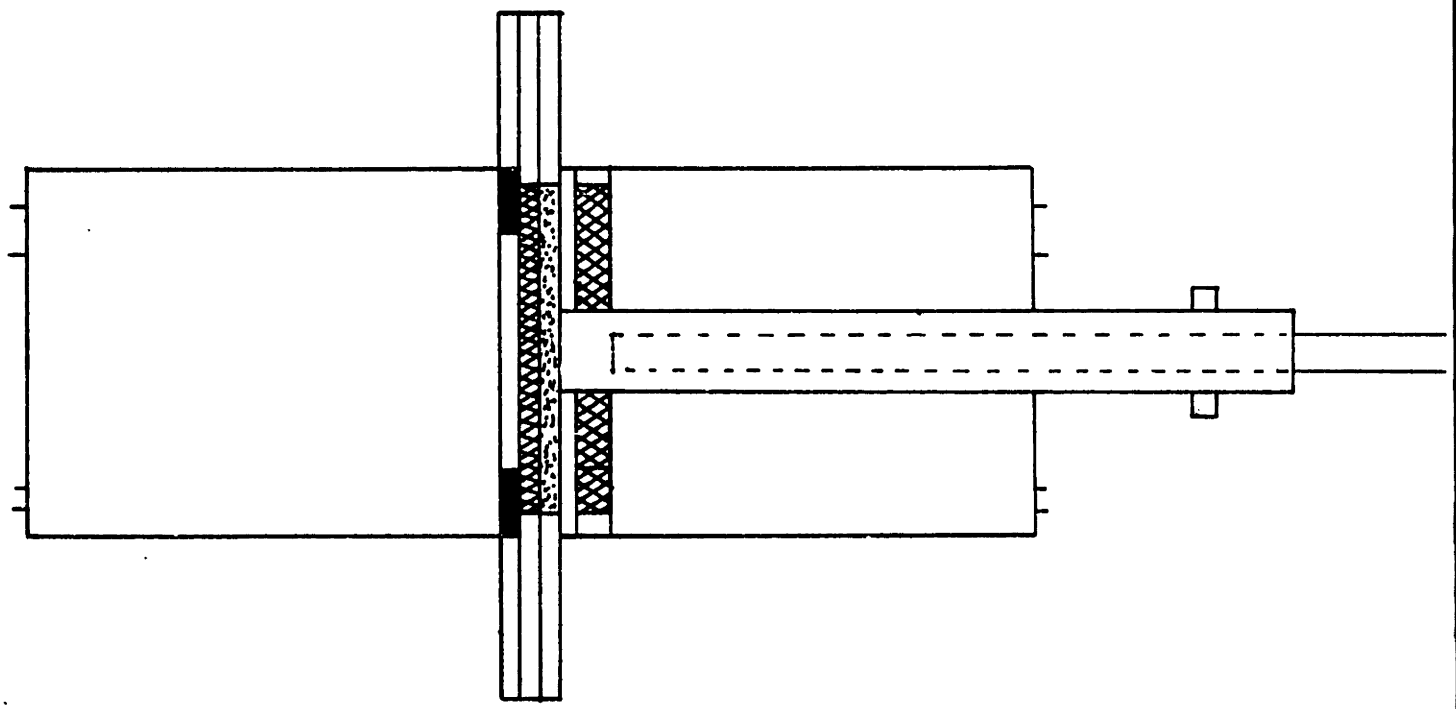

SIDE VIEW

Figure 14

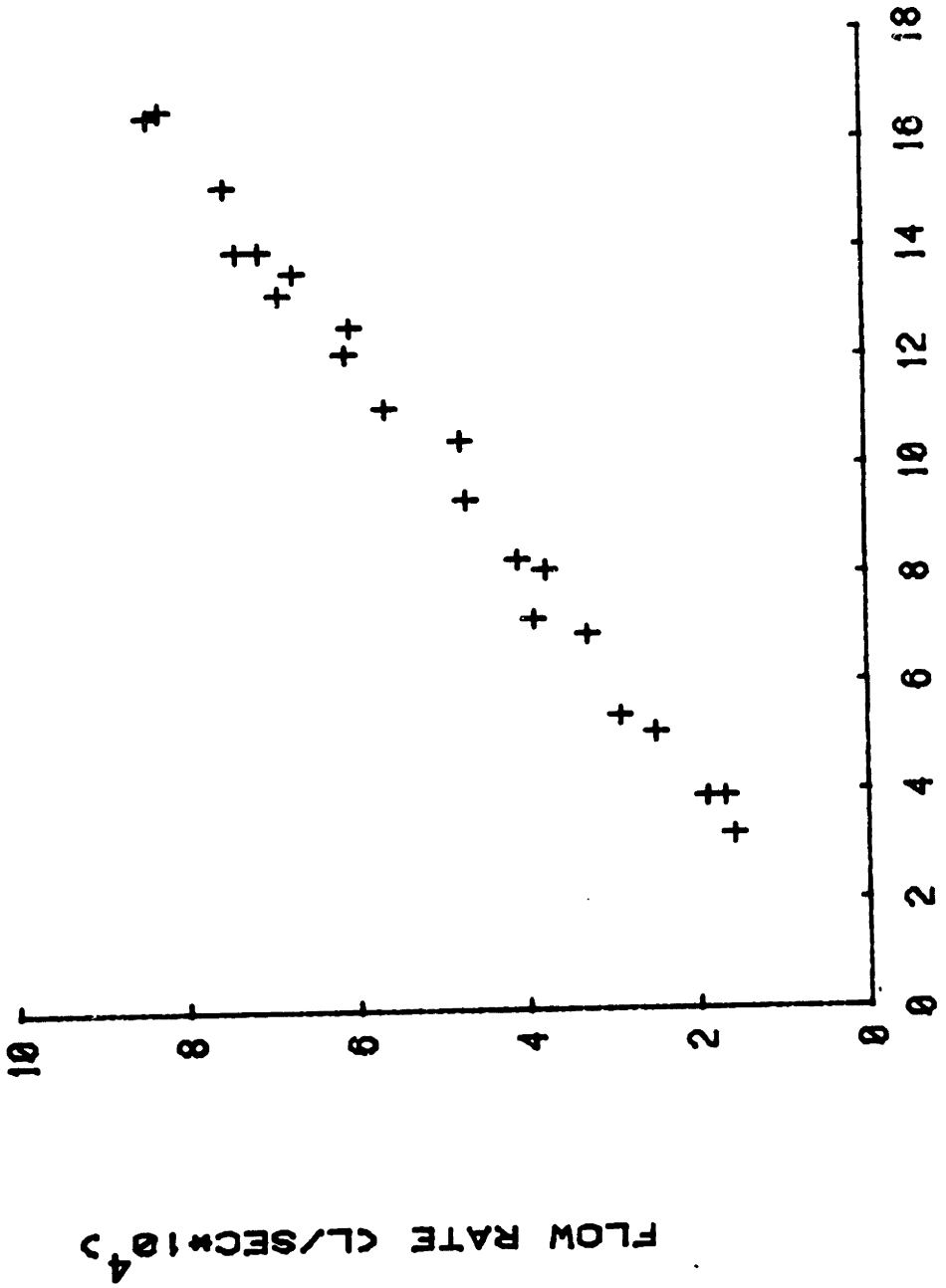
FLOW RATE (L/SEC*10^4)
10
8
6
4
2
0
0
2
4
6
8
10
12
14
16
18
PRESSURE DROP (CM)

Figure 15

(a)

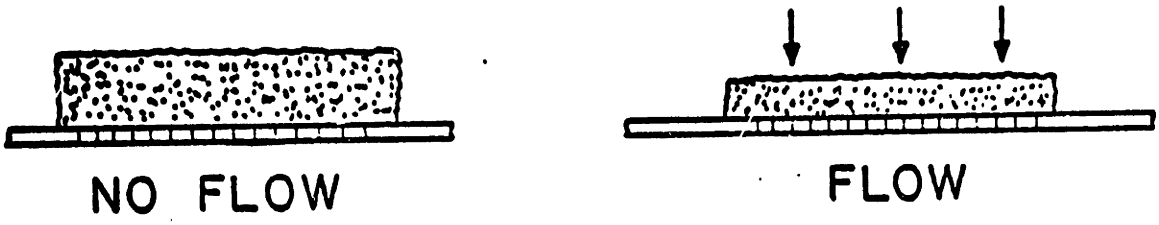

(b)

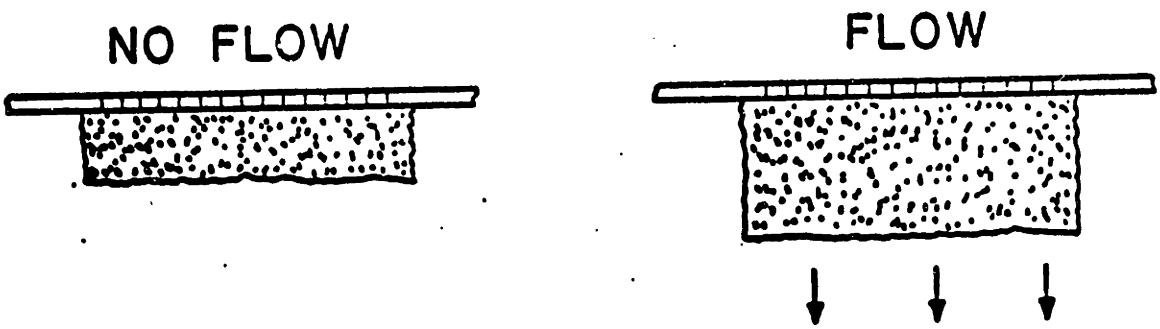

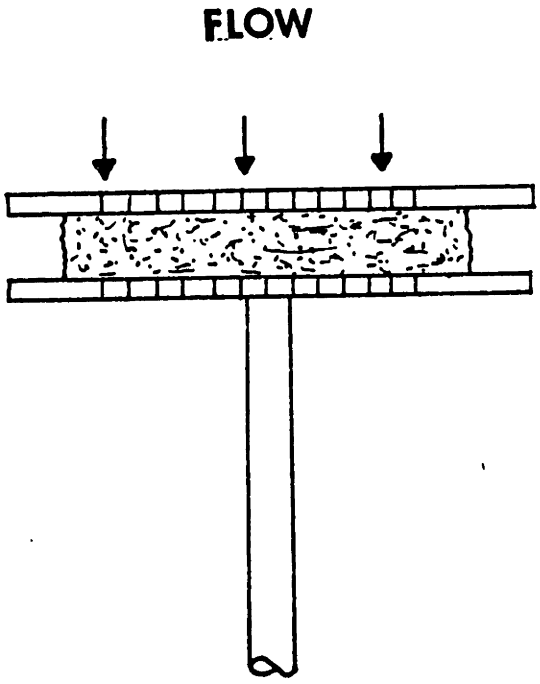

Figure 16

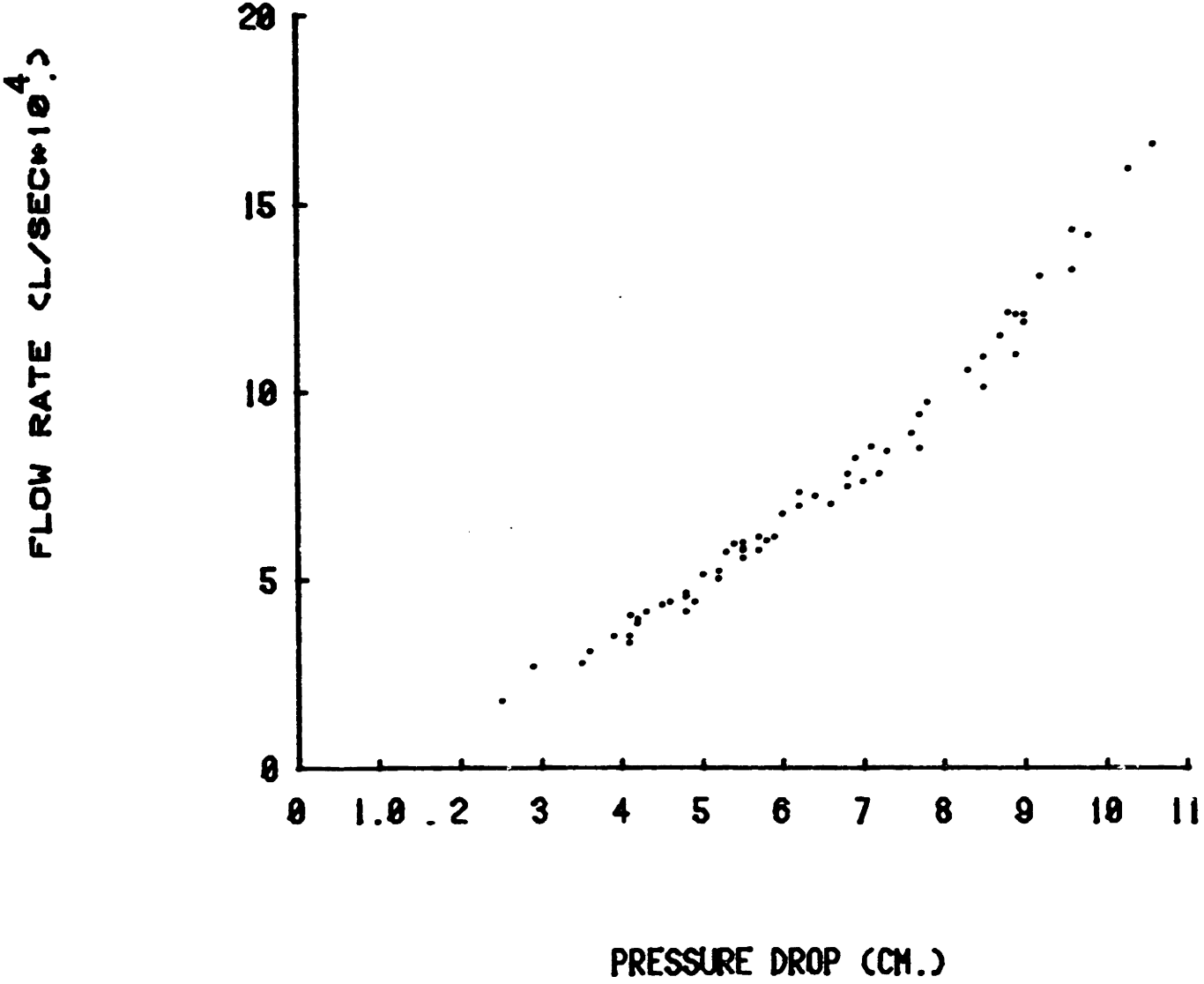
FLOW RATE (L/SEC*10^4.)
20
15
10
5
0
0 1.0 .2 3 4 5 6 7 8 9 10 11
PRESSURE DROP (CM.)

Figure 17

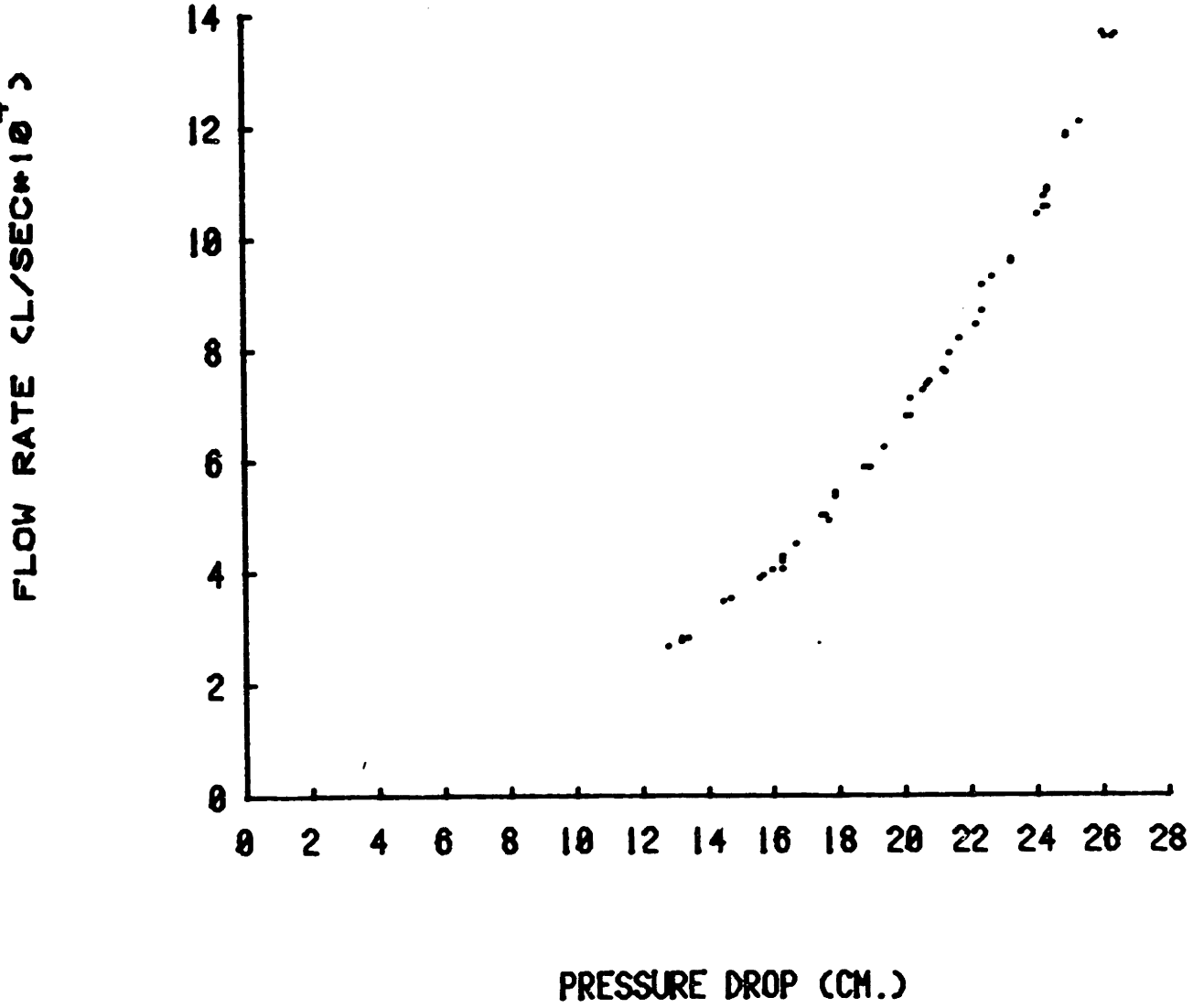
FLOW RATE (L/SEC*10^4)
14
12
10
8
6
4
2
0
0 2 4 6 8 10 12 14 16 18 20 22 24 26 28
PRESSURE DROP (CM.)

Figure 18

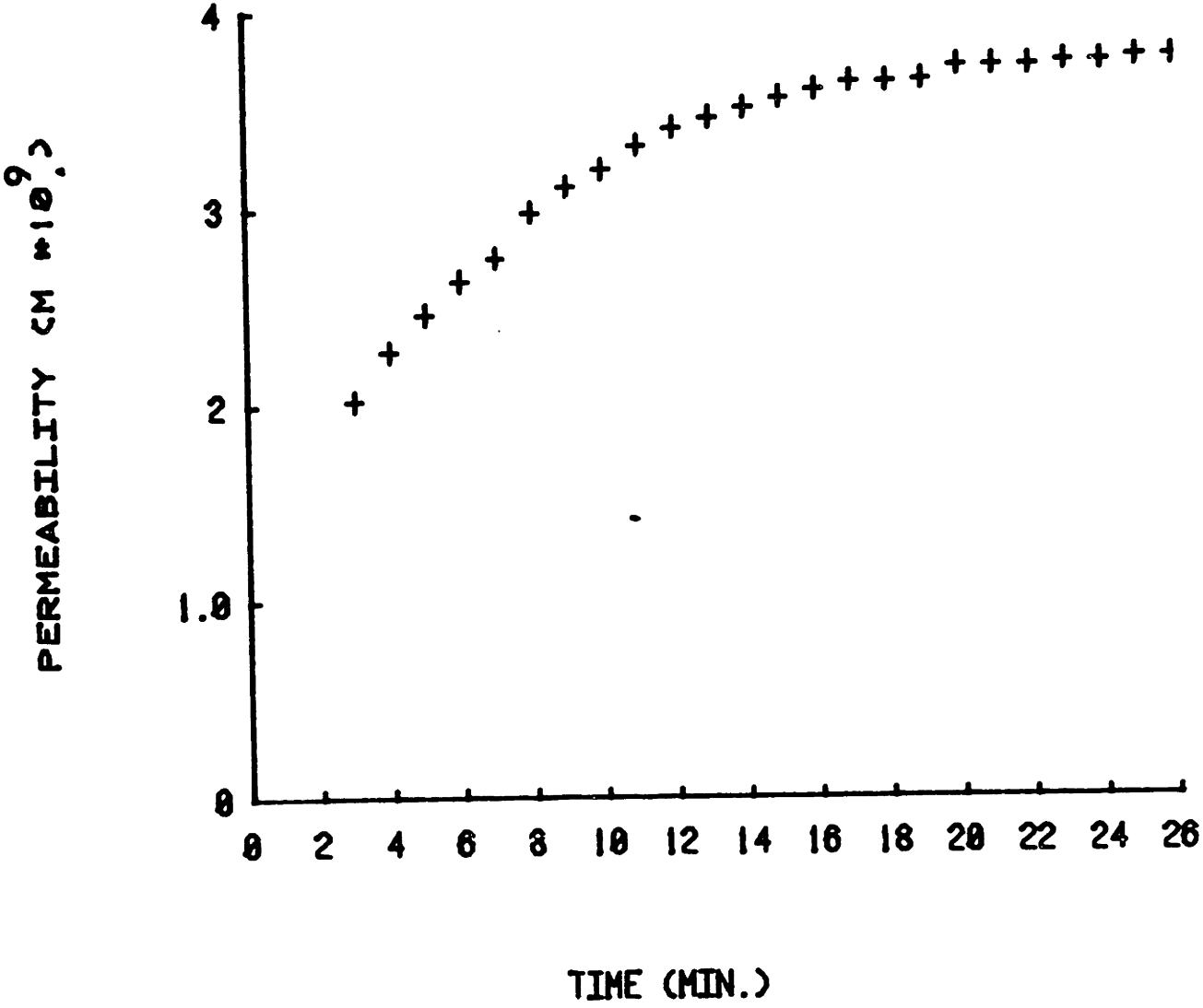
PERMEABILITY (M *10^9.)
4
3
2
1.0
0
0 2 4 6 8 10 12 14 16 18 20 22 24 26
TIME (MIN.)

Figure 19

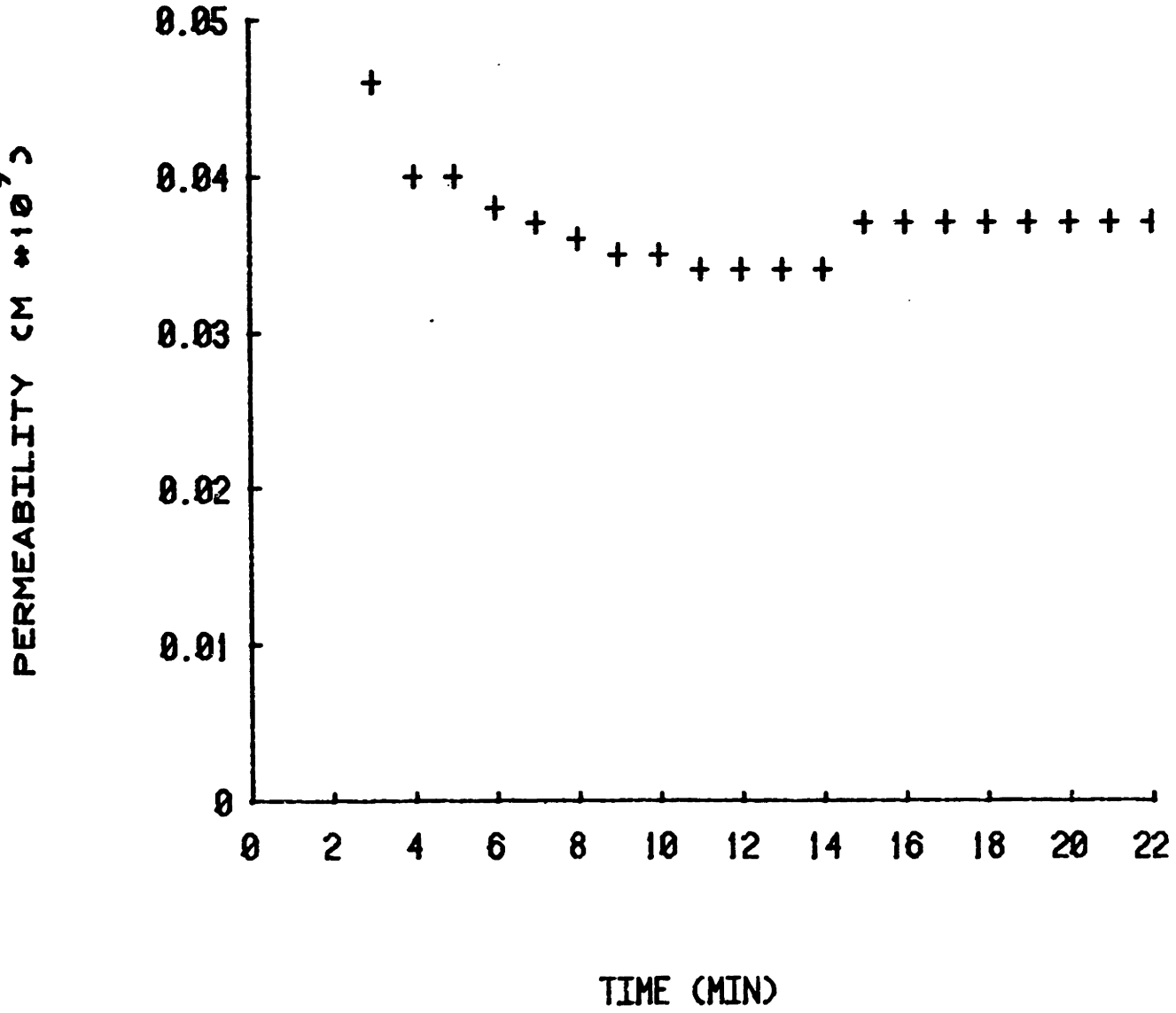
PERMEABILITY (M *10^9)
0.05
0.04
0.03
0.02
0.01
0
0 2 4 6 8 10 12 14 16 18 20 22
TIME (MIN)

Figure 20

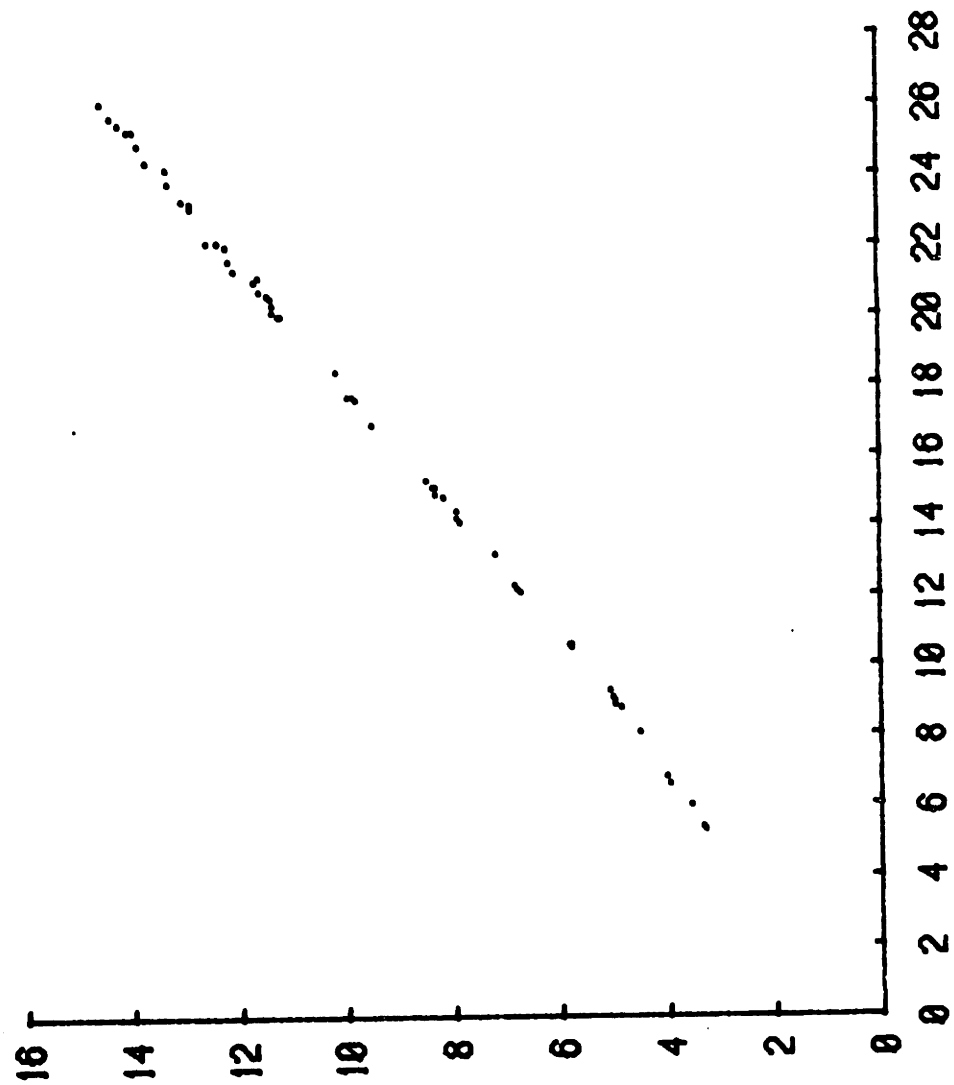
FLOW RATE (L/SEC*10^4)
16
14
12
10
8
6
4
2
0
0 2 4 6 8 10 12 14 16 18 20 22 24 26 28
PRESSURE DROP (CM)

Figure 21

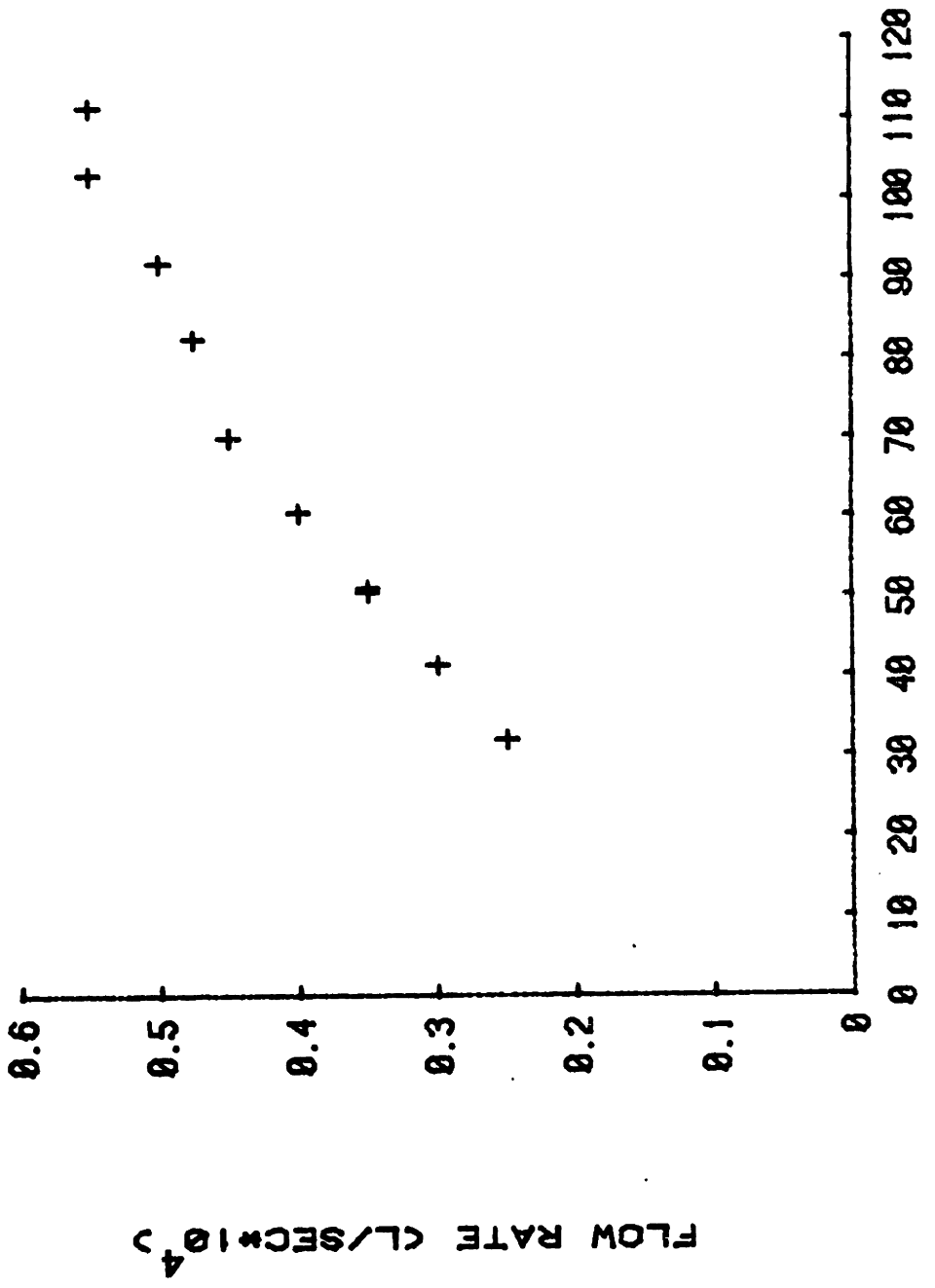
FLOW RATE (L/SEC*10^4)
0.6
0.5
0.4
0.3
0.2
0.1
0
0 10 20 30 40 50 60 70 80 90 100 110 120
PRESSURE DROP (CM)

Figure 22

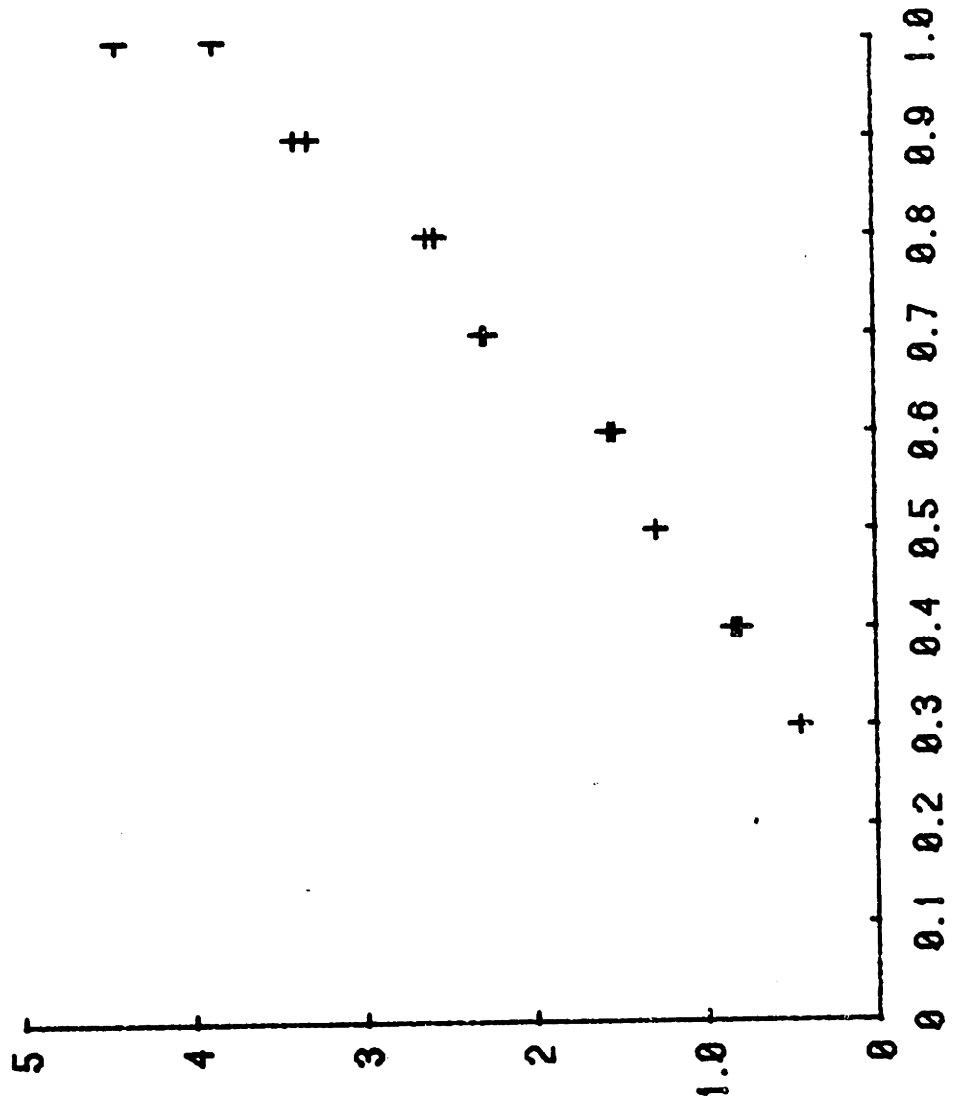
PERMEABILITY CM *10^6
5
4
3
2
1.0
0
0 0.1 0.2 0.3 0.4 0.5 0.6 0.7 0.8 0.9 1.0
COMPRESSION RATIO

Figure 23

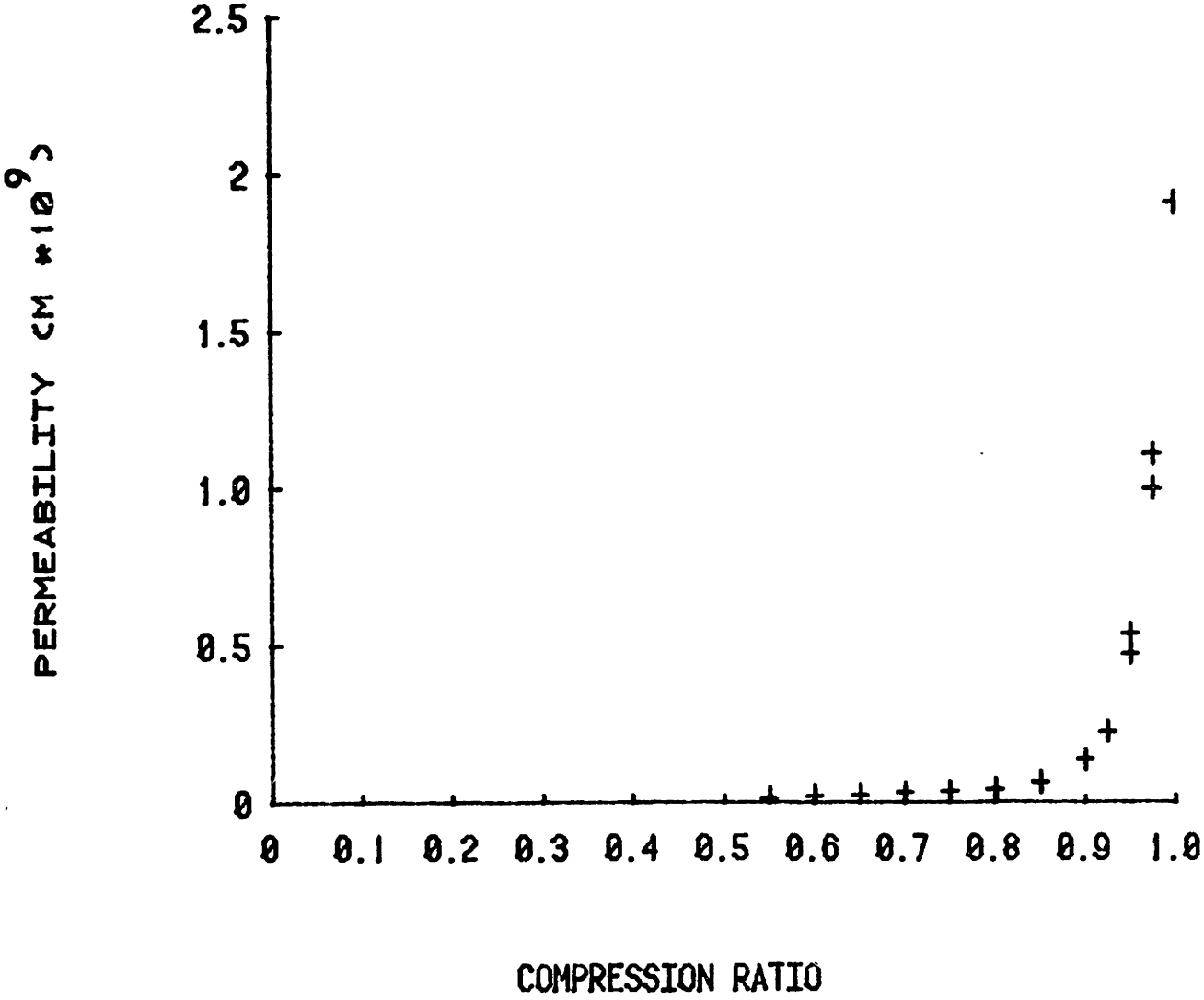
PERMEABILITY CM *10^9>
2.5
2
1.5
1.0
0.5
0
0 0.1 0.2 0.3 0.4 0.5 0.6 0.7 0.8 0.9 1.0
COMPRESSION RATIO

Figure 24

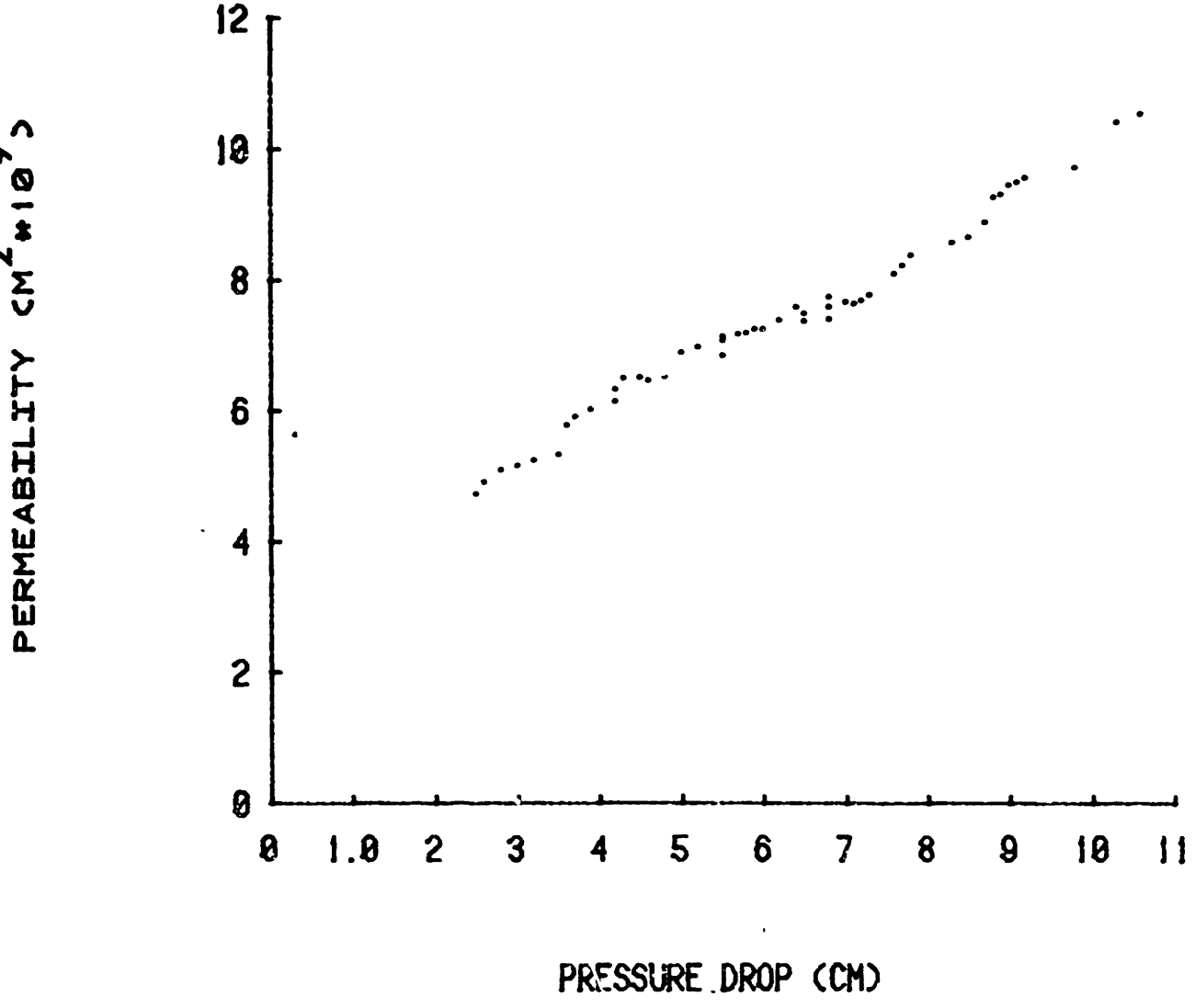
PERMEABILITY (CM^2*10^9)
12
10
8
6
4
2
0
0
1.0
2
3
4
5
6
7
8
9
10
11
PRESSURE DROP (CM)

Figure 25

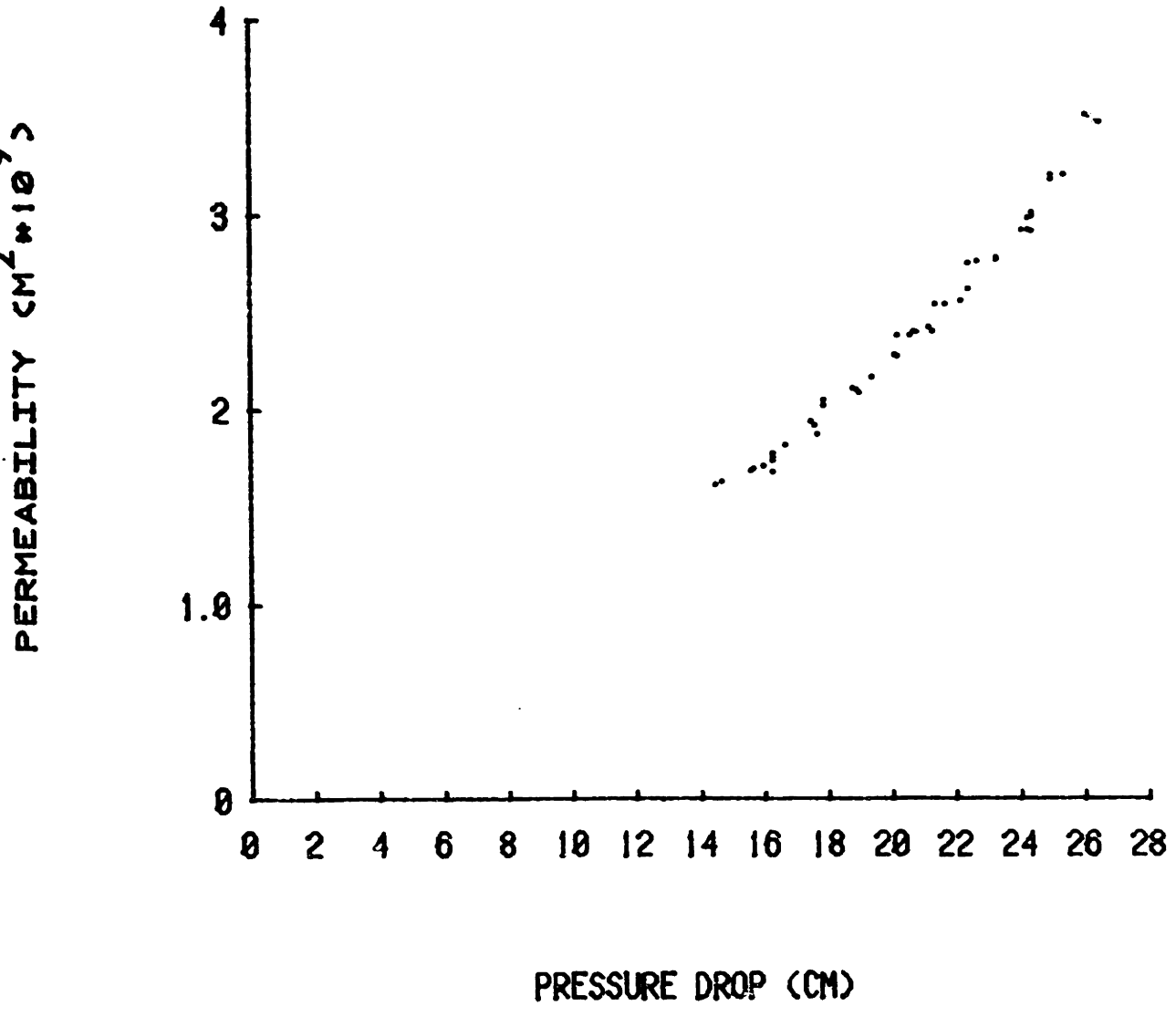
PERMEABILITY (M2*10 9)
4
3
2
1.0
0
0 2 4 6 8 10 12 14 16 18 20 22 24 26 28
PRESSURE DROP (CM)

Figure 26

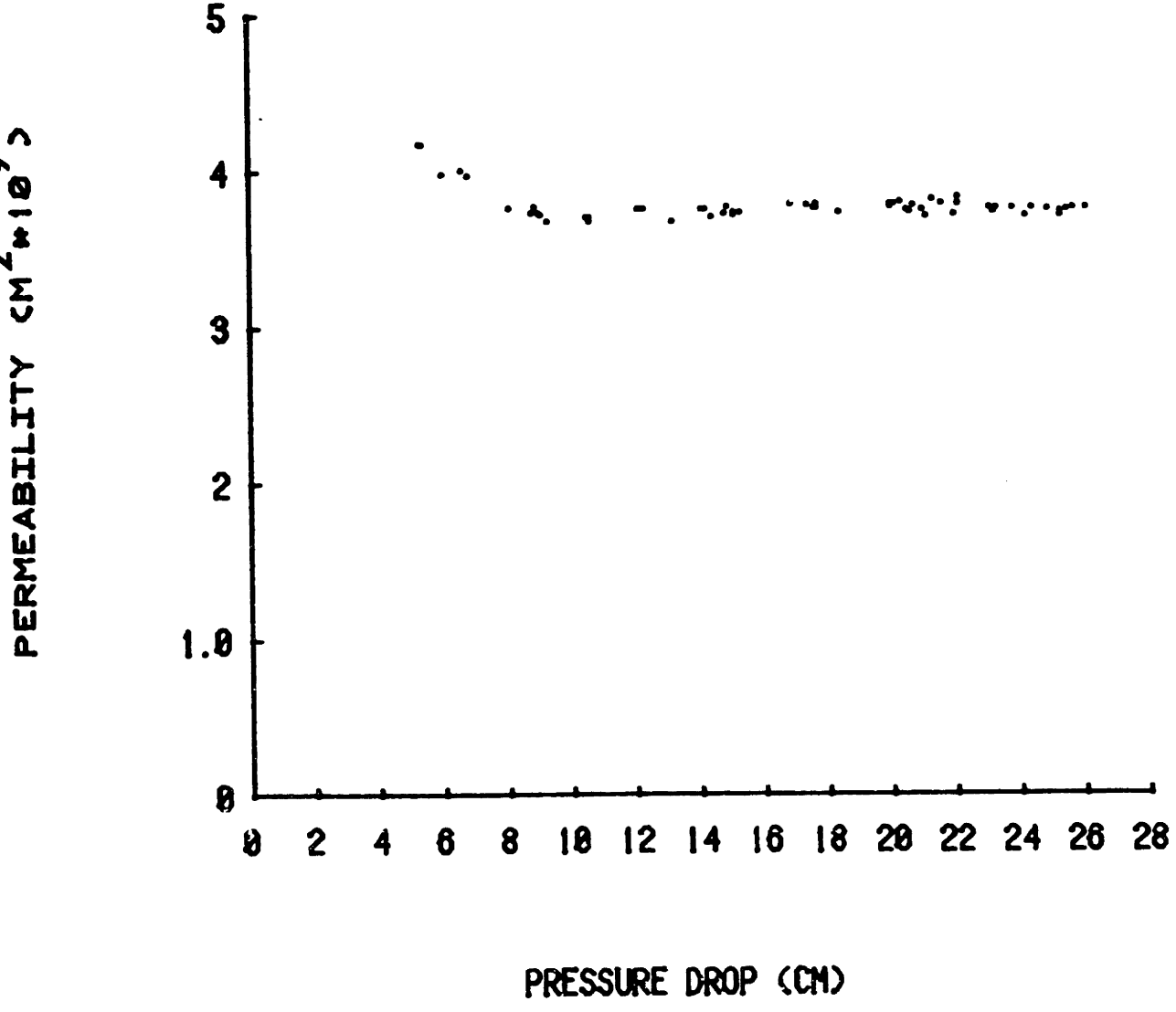
PERMEABILITY (CM^2*10^9)
5
4
3
2
1.0
0
0 2 4 6 8 10 12 14 16 18 20 22 24 26 28
PRESSURE DROP (CM)

Figure 27

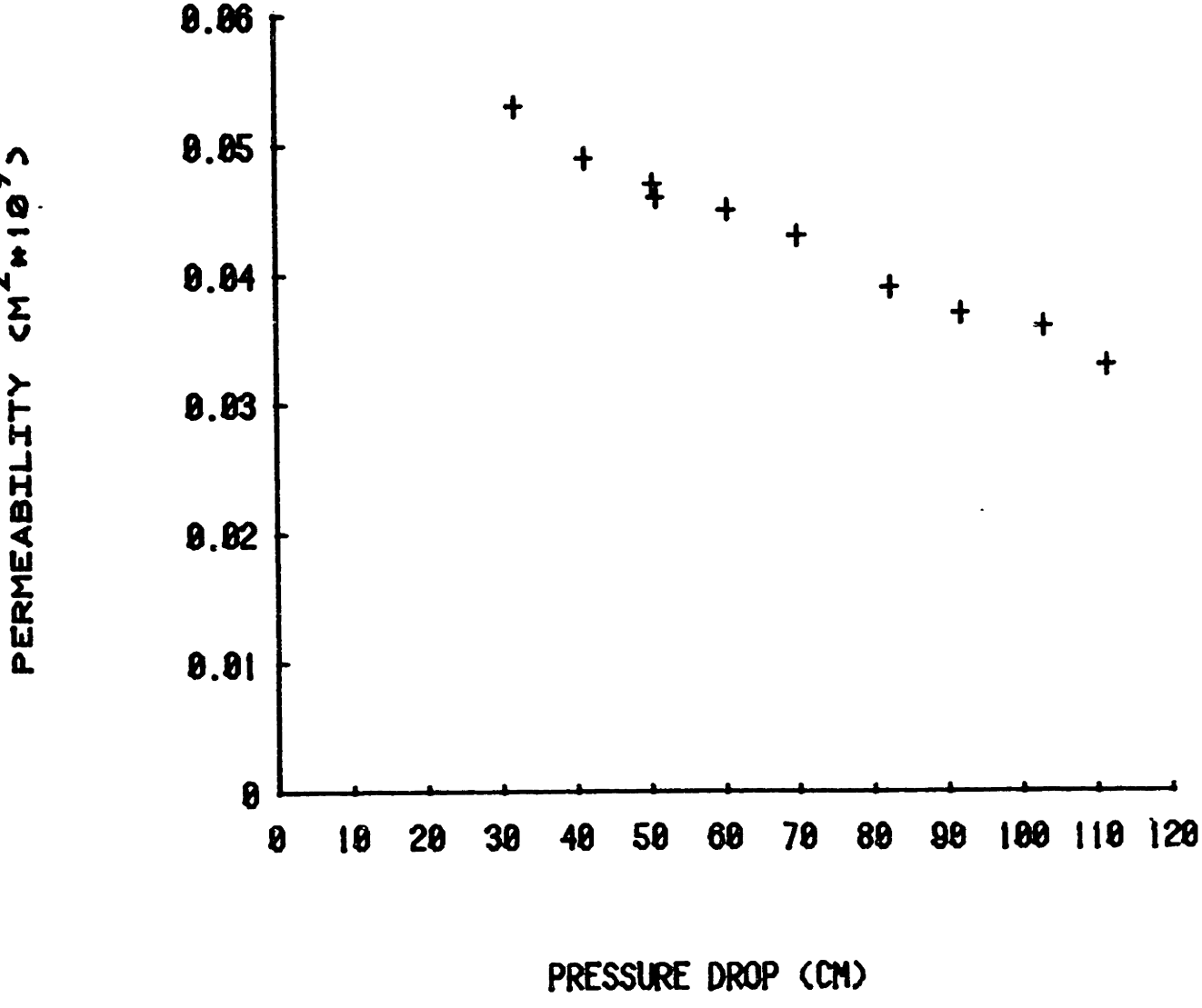
PERMEABILITY (M^2*10^9)
0.06
0.05
0.04
0.03
0.02
0.01
0
0 10 20 30 40 50 60 70 80 90 100 110 120
PRESSURE DROP (CM)

Figure 28

$\lambda = 1$

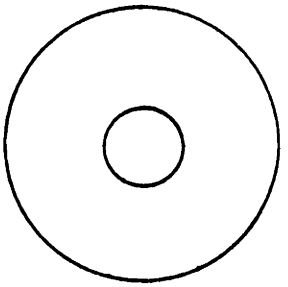

$\lambda = .55$

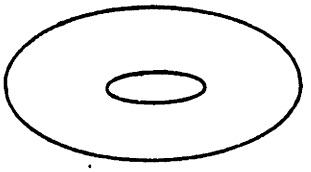

2 P.C.F. FOAM

$\lambda = 1$

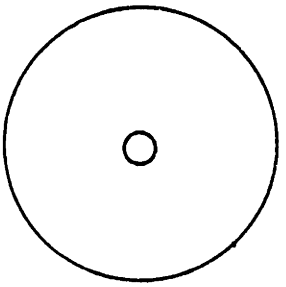

$\lambda = .55$

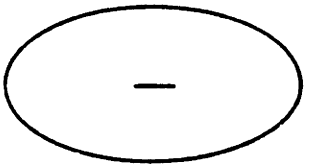

6 P.C.F. FOAM

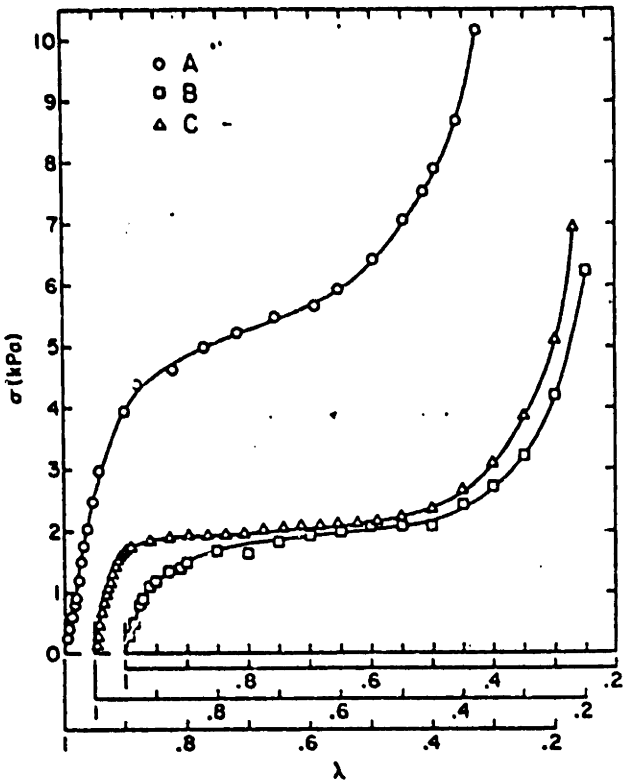

Fig. 2 Stress-deformation characteristics of the deformable porous media (uncertainty of ordinate variable ± 2 percent; uncertainty of abscissa variable ± 0.5 percent)

Figure 30

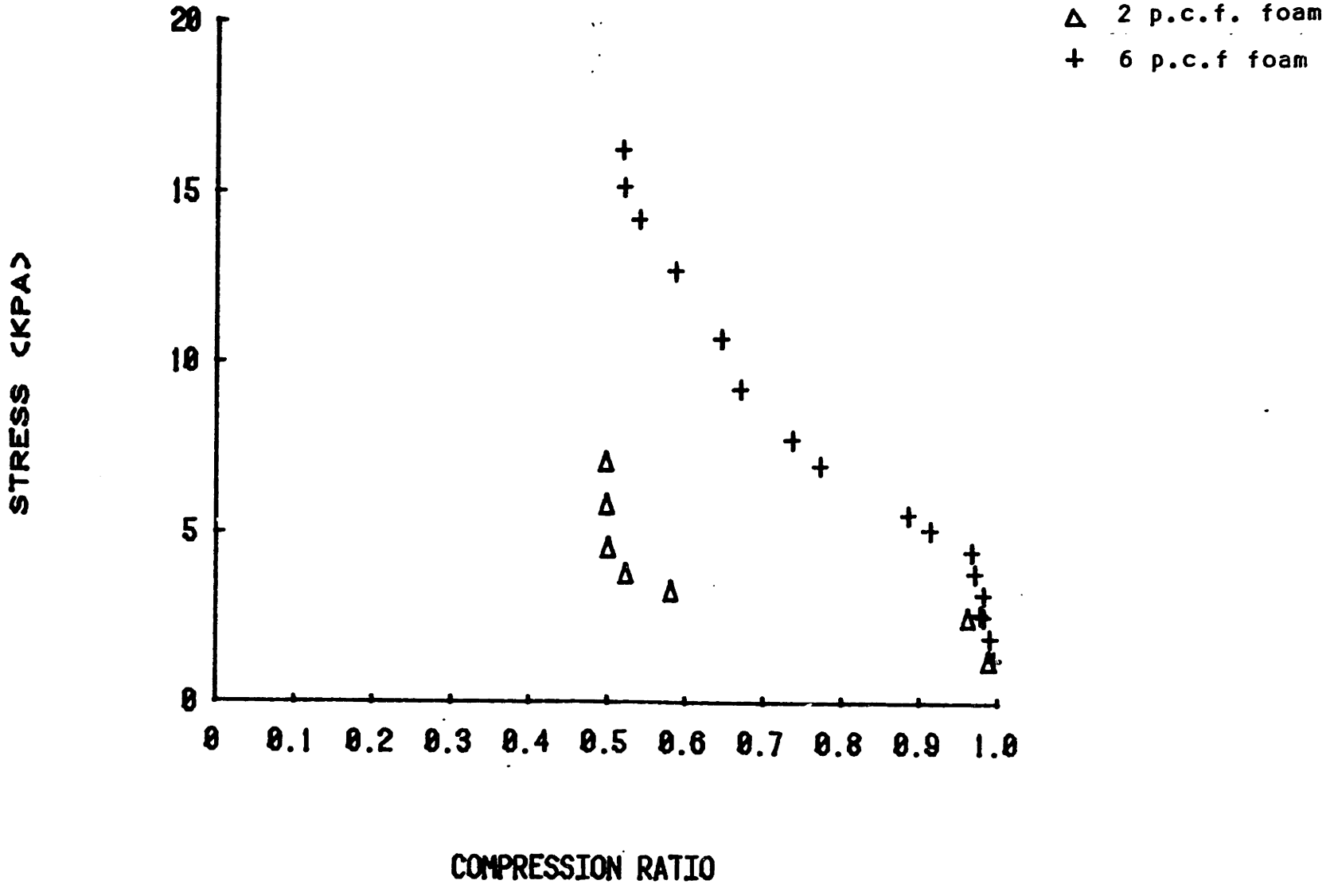
Δ 2 p.c.f. foam
+ 6 p.c.f foam
STRESS (KPA)
20
15
10
5
0
0 0.1 0.2 0.3 0.4 0.5 0.6 0.7 0.8 0.9 1.0
COMPRESSION RATIO

Figure 31

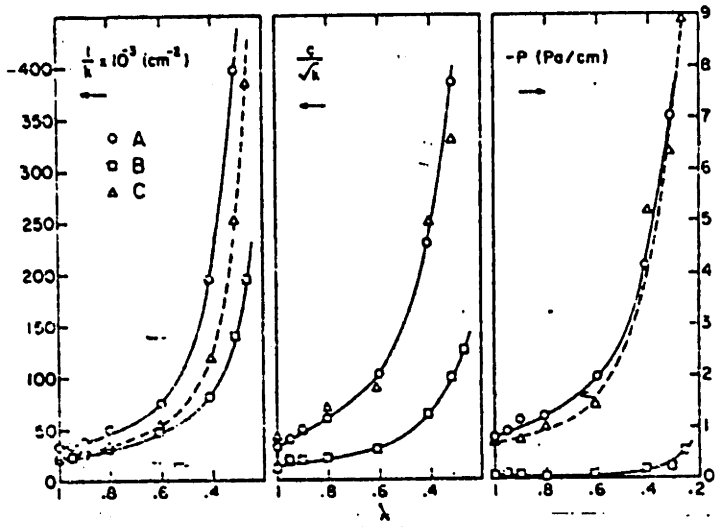

Fig. 5 Experimentally determined flow parameters of the deformable porous media (uncertainty of ordinate variable ± 5 percent; uncertainty of abscissa variable = 0.5)

Figure 32

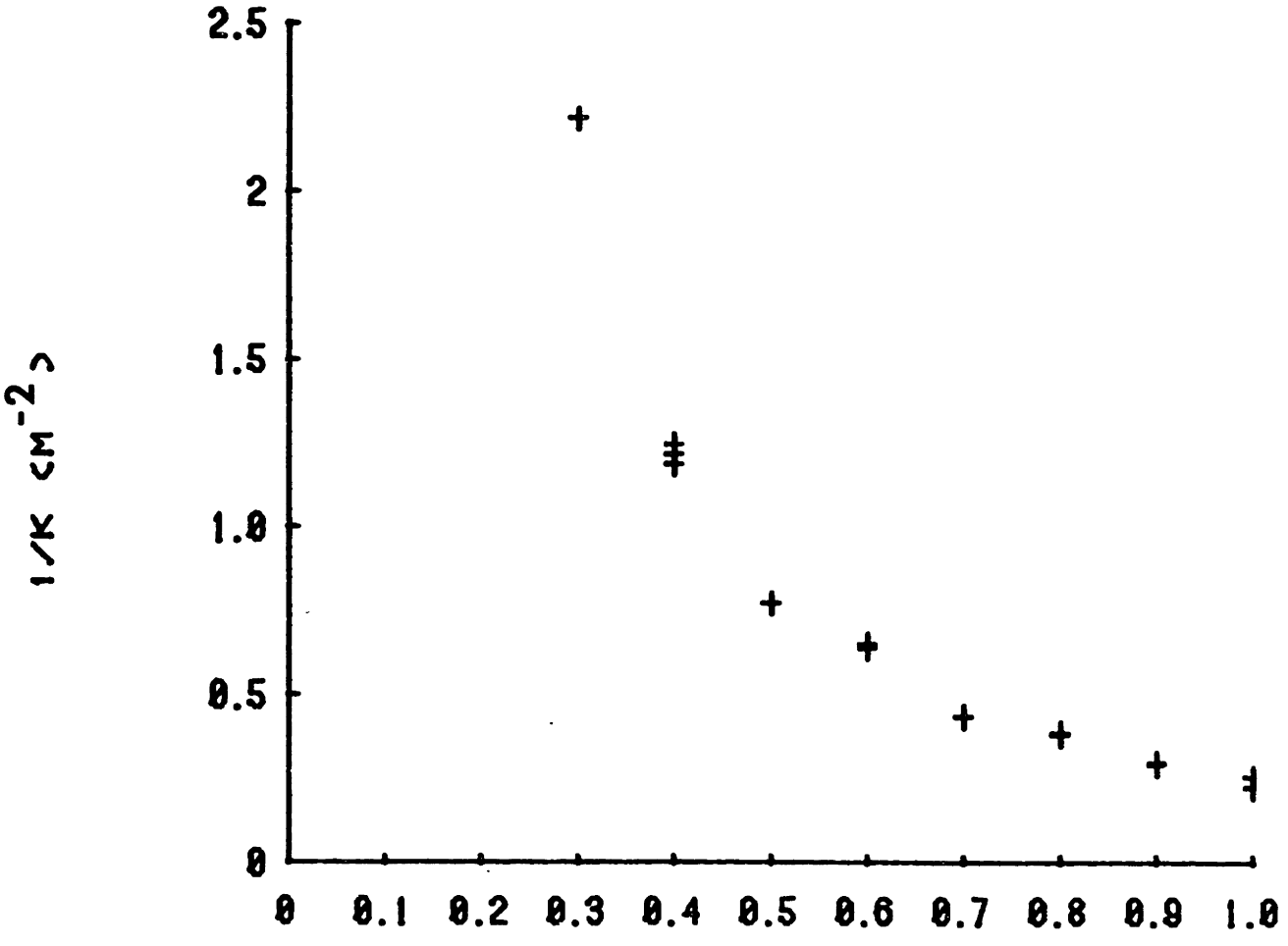
2.5
2
1.5
1.0
0.5
0
1/K <M^-2>
0
0.1
0.2
0.3
0.4
0.5
0.6
0.7
0.8
0.9
1.0
COMPRESSION RATIO

Figure 33

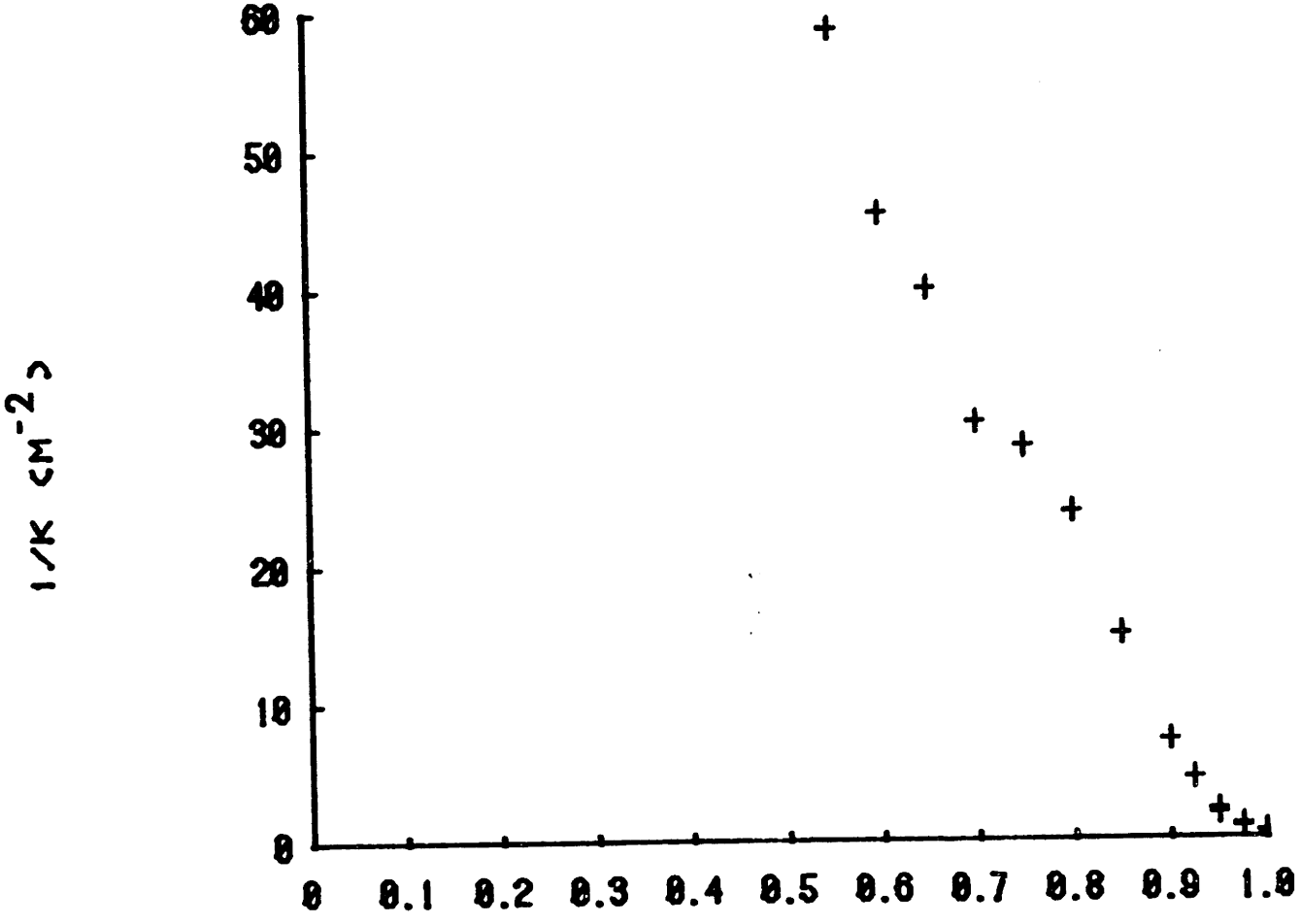
60
50
40
30
20
10
0
1/K (M^-2)
0
0.1
0.2
0.3
0.4
0.5
0.6
0.7
0.8
0.9
1.0
COMPRESSION RATIO

Figure 34

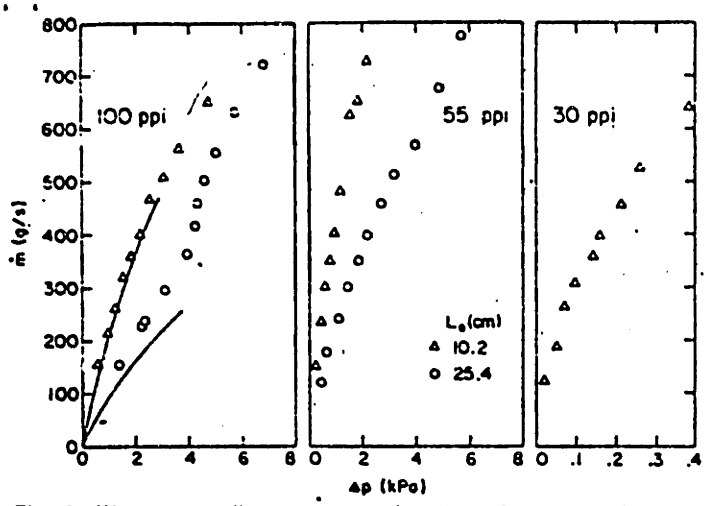

Fig. 6 Water mass flow rate as a function of pressure drop (uncertainty of ordinate variable ± 1 percent; uncertainty of abscissa variable ± 1 percent). The solid lines in the left-hand panel represent the predictions of the analytical model.

Figure 35